ASC Report No. 13/2008

Optimal Convergence of Higher Order Finite Element Methods for Elliptic Interface Problems

Jingzhi Li, Jens Markus Melenk, Barbara Wohlmuth, Jun Zou

Institute for Analysis and Scientific Computing
Vienna University of Technology — TU Wien
www.asc.tuwien.ac.at ISBN 978-3-902627-00-1

Most recent ASC Reports

12/2008 *Samuel Ferraz-Leite, Christoph Ortner, Dirk Praetorius*
Adaptive Boundary Element Method: Simple Error Estimators and Convergence

11/2008 *Gernot Pulverer, Gustaf Söderlind, Ewa Weinmüller*
Automatic Grid Control in Adaptive BVP Solvers

10/2008 *Othmar Koch, Roswitha März, Dirk Praetorius, Ewa Weinmüller*
Collocation Methods for Index 1 DAEs with a Singularity of the First Kind

09/2008 *Anton Arnold, Eric Carlen, Qiangchang Ju*
Large-Time Behavior on Non-Symmetric Fokker-Planck Type Equations

08/2008 *Jens Markus Melenk*
On the Convergence of Filon Quadrature

07/2008 *Dirk Praetorius, Ewa Weinmüller, Philipp Wissgott*
A Space-Time Adaptive Algorithm for Linear Parabolic Problems

06/2008 *Bilgehan Karabay, Gernot Pulverer, Ewa Weinmüller*
Foreign Ownership Restrictions: A Numerical Approach

05/2008 *Othmar Koch*
Approximation of Meanfield Terms in MCTDHF Computations by H-Matrices

04/2008 *Othmar Koch, Christian Lubich*
Analysis and Time Integration of the Multi-Configuration Time-Dependent Hartree-Fock Equations in Electronic Dynamics

03/2008 *Matthias Langer, Harald Woracek*
Dependence of the Weyl Coefficient on Singular Interface Conditions

Institute for Analysis and Scientific Computing
Vienna University of Technology
Wiedner Hauptstraße 8–10
1040 Wien, Austria

E-Mail: admin@asc.tuwien.ac.at
WWW: http://www.asc.tuwien.ac.at
FAX: +43-1-58801-10196

ISBN 978-3-902627-00-1

ASC TU WIEN

Optimal Convergence of Higher Order Finite Element Methods for Elliptic Interface Problems

Jingzhi Li* Jens Markus Melenk† Barbara Wohlmuth‡ Jun Zou§

January 16, 2009

Abstract

Higher order finite element methods are applied to 2D and 3D second order elliptic interface problems with smooth interfaces, and their convergence is analyzed in the H^1- and L^2-norm. The error estimates are expressed explicitly in terms of the approximation order p and a parameter δ that quantifies the mismatch between the smooth interface and the finite element mesh. Optimal H^1- and L^2-norm convergence rates in the entire solution domain are established when the mismatch between the interface and mesh is sufficiently small. Furthermore, under weaker conditions on the mismatch between the interface and mesh, optimal estimates are obtained in an H^1-norm that excludes a thin tubular neighborhood of the interface. For some typical cases of meshes where the interface is approximated by a spline, the mismatch δ is expressed in terms of the order of the spline. The resulting error estimate is then explicit in the approximation order and the order of the spline. Five numerical examples are presented to illustrate and confirm the sharpness of the approximation theory.

Key words. Elliptic interface problems, blending finite element, higher order finite elements, optimal convergence.

AMS subject classification. 65N12, 65N30

1 Introduction

Elliptic interface problems are frequently encountered in scientific computing and industrial applications [19]. A typical example is provided by the modelling of physical processes which involve two or more materials with different properties, such as the conductivity of steel and

*Department of Mathematics, The Chinese University of Hong Kong, Shatin, N.T., Hong Kong (jzli@math.cuhk.edu.hk). The work of this author was in part supported by the German Research Foundation (SPP 1146).

†Institut für Analysis und Scientific Computing, Technische Universität Wien, Austria (melenk@tuwien.ac.at).

‡Institut für Angewandte Analysis und Numerische Simulation (IANS), Universität Stuttgart, 70569 Stuttgart, Germany (wohlmuth@ians.uni-stuttgart.de).

§Department of Mathematics, The Chinese University of Hong Kong, Shatin, N.T., Hong Kong (zou@math.cuhk.edu.hk). The work of this author was substantially supported by Hong Kong RGC grants (Projects 404606 and 404105).

bronze in heat diffusion. It is well-known that the solutions of elliptic interface problems may have higher regularity in each individual material region than the regularity in the entire physical domain due to the discontinuity of material properties across the interface.

Numerous numerical methods for elliptic interface problems with arbitrary but smooth interfaces have been extensively studied during the last two decades; we refer to [2–4, 6–8, 14, 15, 18, 20, 21], the recent monograph [19], and the references therein for an overview. Roughly speaking, these methods can be categorized into three classes, namely, *conforming*, *nonconforming* and *IIM-related*. For conforming methods, mostly linear finite element approximations have been studied with the interface being approximated by a linear interpolating spline (see [2–4, 7, 21]); isoparametric elements have also been analyzed in [3]. Nonconforming methods include mortar element method [15], Nitsche's method [14], which is closely related to DG-type methods, and an interior penalty stabilized Lagrange multiplier method [6]. In view of the effectiveness of the immersed interface methods for rectangular domains, immersed FEMs of linear and quadratic classes in 1D and 2D on Cartesian grids are constructed and analyzed in [8, 18, 20].

The current work is concerned with the analysis of conforming higher order FEMs for two- and three-dimensional interface problems with smooth interfaces. If the interface is resolved exactly (e.g., using blending element techniques in [11–13]), then optimal rates of convergence can be expected in appropriate Galerkin settings. But it is in general impractical to resolve the curved interface exactly in numerical implementations, and the interface has to be approximated. In this case, the mismatch between the FEM mesh and the interface raises several questions:

1. How does the approximation of the interface affect the approximation properties of FEM spaces? More precisely, how accurate should the approximation of the interface be in order to retain optimal rates of convergence (in H^1 and/or L^2) of higher order FEMs?
2. How should the exact stiffness matrix (and the load vector involving the interface source term) be effectively approximated while still preserving optimal rates of convergence? This is an important issue in implementations since it is unrealistic to evaluate the stiffness matrix (and the load vector) exactly in view of the fact that the coefficients of the differential equation are not necessarily smooth on elements near the interface. Hence, the exact bilinear form a (likewise the right-hand side) has to be approximated by a computationally tractable one a_h, and the effect of this variational crime has to be appropriately controlled.
3. To what extent is the error introduced by approximating the interface localized? That is, is the error due to this approximation (essentially) restricted to a small vicinity of the interface?

The purpose of this present work is to provide answers to the above three questions. Theorems 4.2, 4.6 and the discussion in Section 4.3 will address the first two questions, and provide convergence results for p-th order FEMs under the assumption that the mesh resolves the interface up to an order $O(\delta)$ (see Def. 3.1 for a precise definition). As an example, we mention that one may expect $\delta = O(h^{m+1})$ if an interface is approximated in 2D by an interpolating spline of degree m. In this situation the error of the FEM is $O(h^{\min\{p,(m+1)/2\}})$ in H^1 and $O(h^{\min\{p,m\}+1})$ in L^2 (given sufficient regularity). In particular, we obtain optimal convergence rates both in H^1 and L^2 for piecewise linear elements ($p = 1$) and piecewise linear interpolation of the interface ($m = 1$). We would like to emphasize that for $p > 1$ the conditions on the interface approximation are more stringent for optimal convergence rates in H^1 than for opti-

mal convergence rates in L^2. These stringent conditions can be relaxed by adopting a different error measure, for example, by restricting the attention to the convergence of the FEM away from the interface. In doing so, Section 4.4 addresses the aforementioned third question. We will show in Theorem 4.14 that optimal H^1-convergence can be achieved *outside* a thin tubular neighborhood of the interface under significantly weaker conditions on the mismatch between the interface. Returning to the 2D example of an interpolating spline of degree m discussed above, the FEM error is $O(h^{\min\{p,m\}})$ when measured in the norm of $H^1(\Omega \setminus S_\delta)$, where S_δ is a tubular neighborhood of the interface of width $\delta = O(h^{m+1})$.

The present work is closely related to the earlier works [3, 4, 7]. The work [3] analyzes the case of *isoparametric* elements and obtains optimal convergence rates under extra regularity assumptions (see [3, Thm. 2.1]). References [4, 7] restrict their attention to the 2D case. In all three references, the interface is approximated by an interpolating spline (possibly of higher order); in contrast, the present paper does not make this assumption and merely requires the approximation to the interface to be sufficiently accurate in an appropriate sense (see Def. 3.1).

Although the detailed approximation theory is developed in this work only for a scalar elliptic model problem, analogous results can be naturally extended to some vectorial systems such as the Lamé equations; a numerical example is presented to illustrate this point in Section 5.

The rest of the paper is organized as follows. In Section 2, we introduce the triangulation of the domain and finite element spaces, where an abstract framework is adopted in which very weak approximation properties and conditions on the element maps are stipulated. Using this framework, the classical affine elements, curved elements [9, 24] and blending elements can be treated in a unified manner. Section 3 analyzes the approximation of piecewise smooth functions by FEM spaces, with special attention to the mismatch between the mesh and the interface. The basic analysis tools are a *δ-strip* argument (Lemma 3.4) as well as a modified nodal interpolation operator (Def. 3.3). The approximation results of Section 3 are applied to the FEM in Section 4, and optimal convergence results both in H^1 and L^2 are obtained. Five numerical examples are presented in Section 5 to illustrate and confirm the effectiveness and sharpness of the approximation theory developed in this work.

2 Elliptic interface problem and FEM spaces

In this work we will develop a general convergence theory for finite element methods for elliptic interface problems. For the sake of exposition, we will focus our theory on the following model elliptic interface problem:

$$-\nabla \cdot (\beta \nabla u) = f \quad \text{in } \Omega\,, \tag{1}$$

which is complemented with the Dirichlet boundary condition

$$u = 0 \quad \text{on } \partial\Omega \tag{2}$$

and the jump conditions on the interface for the solution and the flux:

$$[u] = 0 \quad \text{on } \Gamma, \qquad \left[\beta \frac{\partial u}{\partial \mathbf{n}}\right] = g \quad \text{on } \Gamma\,. \tag{3}$$

The domain Ω is assumed to be occupied by two different media or materials, Ω_1 and Ω_2, with $\Omega_1 \subset\subset \Omega$, $\Omega_2 := \Omega \setminus \overline{\Omega}_1$, and the interface $\Gamma := \partial\Omega_1$ (see Fig. 1) is required to have at least C^2-regularity and $f \in L^2(\Omega)$ and $g \in H^{1/2}(\Gamma)$. The positive coefficient function β is assumed

to be piecewise constant, i.e., there exists two positive number $\beta_i > 0$, $i = 1, 2$ such that $\beta|_{\Omega_i} = \beta_i$, $i = 1, 2$.

We assume at this point $\Omega \subset \mathbb{R}^d$ to be a Lipschitz domain. The conditions on the triangulation will effectively impose that $\partial\Omega$ be piecewise smooth.

In the rest of this section we introduce some notations and conventions that will be used throughout the work. The vector $\mathbf{n}$ is always understood to be the unit outward normal to the boundary $\partial\Omega_1$. For a function $u \in L^2(\Omega)$ we denote by u_i its restriction on Ω_i, i.e., $u_i := u|_{\Omega_i}$. The jump $[v]$ is always understood to be $v_1 - v_2$ on Γ. We restrict our attention here to Dirichlet boundary conditions on $\partial\Omega$ and piecewise constant coefficients β; the extension to other boundary conditions such as Neumann conditions and piecewise smooth functions β is possible; see the remarks at the end of Section 4.3.

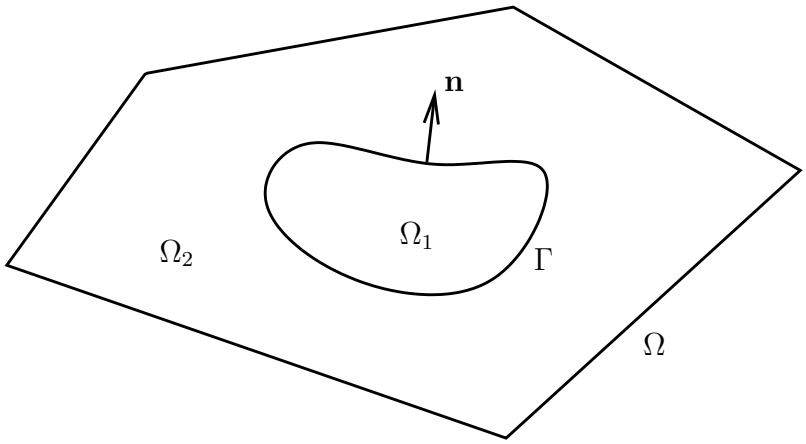

Figure 1: Domain Ω and its subdomains Ω_1 and Ω_2.

For any nonnegative integer k, $H^k(\Omega)$ stands for the standard Sobolev space [1], and $H^1_0(\Omega)$ is the subspace of $H^1(\Omega)$ consisting of all functions that vanish on $\partial\Omega$ in the sense of traces. For any function v defined on Ω_i $(i = 1, 2)$, we will often need its extension to the entire space $\mathbb{R}^d$. This can be achieved with the Stein extension operator $E_i : L^2(\Omega_i) \to L^2(\mathbb{R}^d)$, [22]. We recall that this operator is a bounded linear operator $E_i : H^k(\Omega_i) \to H^k(\mathbb{R}^d)$ for any fixed $k \geq 0$.

As usual, C denotes a generic constant independent of critical parameters such as the mesh size h. For non-negative expressions A, B, the notation $A \lesssim B$ means the existence of a constant $C > 0$ such that $A \leq CB$, where, again, C is independent of the mesh size h.

2.1 Triangulations

We triangulate the domain Ω by a collection of (possibly curved) open simplicial elements K, denoted by $\mathcal{T}$. Each element $K \in \mathcal{T}$ is the image of a standard open unit simplex, the so-called reference element $\widehat{K} \subset \mathbb{R}^d$, under an element map $F_K : \overline{\widehat{K}} \to \overline{K}$. For each element K, the images of faces, edges, vertices of the reference element $\widehat{K}$ under the map F_K are called faces, edges, and vertices of K, respectively. We set $h_K := \operatorname{diam} K$.

The precise conditions on the element maps F_K are formalized in the following definition.

Definition 2.1 (γ-shape regular)**.** *A triangulation $\mathcal{T}$ with corresponding element maps $\{F_K\}_{K\in\mathcal{T}}$ is a* γ-shape regular triangulation *of Ω if the following conditions are satisfied:*

(T1) *The maps* $F_K : \hat{K} \to K = F_K(\hat{K})$ *are* C^1*-diffeomorphisms between* $\overline{\hat{K}}$ *and* $\overline{K}$*, not necessarily affine.*

(T2) $\overline{\Omega} = \cup_{K\in\mathcal{T}}^{N} \overline{K}$*; and for each pair of elements* K*,* K' *from* $\mathcal{T}$ *there holds either* $K = K'$ *or* $K \cap K' = \emptyset$*.*

(T3) *For each pair of elements* K *and* K' *from* $\mathcal{T}$*, the intersection* $\overline{K} \cap \overline{K'}$ *is either empty, or a face, an edge or a vertex shared by* K *and* K'*. If* $\overline{K} \cap \overline{K'} \neq \emptyset$*, then for* $\sigma = \partial K \cap \partial K'$*, the map* $Q : x \mapsto \left(F_{K'}^{-1} \circ F_K\right)(x)$ *is an isometric isomorphism between* $F_{K'}^{-1}(\sigma)$ *and* $F_K^{-1}(\sigma)$*.*

(T4) $\|F_K'\|_{L^\infty(\widehat{K})} \leq \gamma h_K$ *and* $\|(F_K')^{-1}\|_{L^\infty(\widehat{K})} \leq \gamma h_K^{-1}$ *for all* $K \in \mathcal{T}$*.*

Examples of specific choices of the element maps F_K will be discussed in Section 4. In addition to the shape regularity, we will restrict our analysis in this paper to quasiuniform triangulations $\mathcal{T}$ of mesh size h, i.e., the triangulations $\mathcal{T}$ satisfy

$$h_K \leq h \leq C h_K \qquad \forall\, K \in \mathcal{T} \tag{4}$$

for a constant $C > 0$ independent of h.

We point out that Condition (T4) implies that the number of elements that share a node or an edge is bounded by a constant depending solely on γ and is in particular independent of h. From the assumption $h_K \leq h$ we immediately get that $K \subset B_K := B_h(b_K)$, where $B_h(b_K)$ is the ball of radius h centered at the barycenter b_K of K. The γ-shape regularity (Condition (T4)) of the triangulation $\mathcal{T}$ yields directly the existence of $M > 0$ depending solely on γ and the constant C of (4) such that

$$\mathrm{card}\{K \in \mathcal{T}\,; \quad x \in B_K\} \leq M \qquad \forall\, x \in \Omega \tag{5}$$

where $\mathrm{card}(A)$ stands for the number of the elements in a given set A.

Remark 2.2. Condition $(T2)$ in Definition 2.1 requires the triangulation $\mathcal{T}$ to cover Ω exactly. This is done for convenience in order to concentrate on the approximation of the interface Γ. Approximating the outer boundary $\partial\Omega$ introduces additional variational crimes that have, however, already been studied in the literature.

2.2 Finite Element Spaces

Let $\mathcal{T}$ be a γ-shape regular triangulation of Ω, and let $\widehat{P}_p$ be the space of polynomials of total degree less than or equal to p in d variables. Then we define the finite element space

$$S^{p,1}(\mathcal{T}) = \{u \in H^1(\Omega); \quad u|_K \circ F_K \in \widehat{P}_p(\widehat{K}) \quad \forall K \in \mathcal{T}\}\,, \tag{6}$$

and its subspace $S_0^{p,1}(\mathcal{T}) = S^{p,1}(\mathcal{T}) \cap H_0^1(\Omega)$. The approximation theory of Section 3 will be based on nodal finite element interpolation operators mapping from $C(\overline{\Omega})$ to $S^{p,1}(\mathcal{T})$. The first operator I_p is constructed in the standard way as follows: First, we recall that the simplicial reference element of order p is a triple $(\widehat{K}, \widehat{\Xi}_p, \widehat{P}_p)$, where $\widehat{\Xi}_p = \{\widehat{a}_i^p \in \overline{\widehat{K}} \mid i = 1, \ldots, N_p\}$ is a set of $N_p = \dim \widehat{P}_p$ nodal points in $\overline{\widehat{K}}$. For the sake of definiteness, we select for $\widehat{\Xi}_p$ the classical equidistant arrangement given in [9, Formula 2.2.11, pp. 49]. We will denote the standard nodal interpolation operator on the reference element $\widehat{K}$ by $\widehat{I}_p : C(\overline{\widehat{K}}) \to \widehat{P}_p$ and define I_p elementwise by

$$(I_p u)|_K = \left(\widehat{I}_p(u|_K \circ F_K)\right) \circ F_K^{-1} \quad \forall\, K \in \mathcal{T}. \tag{7}$$

Noting that the condition $(T3)$ of Def. 2.1 explicitly requires the parameterizations from two neighboring elements to be the same on their common part and observing that the nodes of $\widehat{\Xi}_p$ are distributed symmetrically on the edges and faces of $\widehat{K}$ we conclude that $I_p : C(\overline{\Omega}) \to S^{p,1}(\mathcal{T})$ and $(I_p u)|_{\partial\Omega} = 0$ if $u|_{\partial\Omega} = 0$. We set $\Xi(\mathcal{T}) := \cup_{K\in\mathcal{T}} F_K(\widehat{\Xi}_p)$ and observe that each element $v \in S^{p,1}(\mathcal{T})$ is uniquely determined by specifying the nodal values $\{v(x) \,|\, x \in \Xi(\mathcal{T})\}$; additionally, $v|_K$ is uniquely determined by prescribing the values $\{v(x) \,|\, x \in F_K(\widehat{\Xi}_p) = \Xi(\mathcal{T}) \cap \overline{K}\}$.

Concerning the approximation properties of I_p we assume throughout the paper

Assumption 2.3. *For $q \in \{0, 1\}$, the interpolant I_p satisfies*

$$\|v - I_p v\|_{H^q(K)} \lesssim h^{p+1-q} \|v\|_{H^{p+1}(K)} \qquad \forall\, v \in H^{p+1}(K). \tag{8}$$

Remark 2.4. Assumption 2.3 is effectively an assumption on the element maps F_K. It is true for affine element maps and element maps used for isoparametric elements.

Assumption 2.3 quantifies the approximation properties of the nodal interpolation operator I_p on each element K under maximal smoothness assumptions. However, the solutions u to (1)–(3) may be less regular. The optimal approximation properties of I_p for sufficiently smooth functions imply that the spaces $S_0^{p,1}(\mathcal{T})$ have optimal approximation properties when approximating functions that have less regularity, more specifically, the operator I_p has optimal approximation properties also for functions with less regularity, as shown in the following lemma.

Lemma 2.5. *If the interpolation operator I_p satisfies Assumption 2.3, then for every $s \in \{1, \ldots, p\}$ and $q \in \{0, 1\}$ there holds*

$$\|u - I_p u\|^2_{H^q(\Omega)} = \sum_{K\in\mathcal{T}} \|u - I_p u\|^2_{H^q(K)} \lesssim h^{2(s+1-q)} \|u\|^2_{H^{s+1}(\Omega)} \quad \forall\, u \in H^{s+1}(\Omega). \tag{9}$$

Proof. We start by noting that the Stein extension operator allows us to assume $u \in H^{s+1}(\mathbb{R}^d)$. By standard approximation results (see, e.g., [5]), there exists a polynomial π of degree s for every element K such that the following simultaneous approximation properties are satisfied:

$$h^{d/2} \|u - \pi\|_{L^\infty(B_K)} + \sum_{t=0}^{s} h^t |u - \pi|_{H^t(B_K)} \lesssim h^{s+1} |u|_{H^{s+1}(B_K)} \tag{10}$$

where B_K is defined in Subsection 2.1. We now employ the estimate (10), Assumption 2.3, an inverse estimate for polynomials (cf. [5, Lemma 4.5.3]), the fact that $K \subset B_K$, and $\pi \in \mathcal{P}_s$ to get for $q \in \{0, 1\}$ that

$$\begin{aligned} |u - I_p u|_{H^q(K)} &\leq |u - \pi|_{H^q(K)} + |\pi - I_p \pi|_{H^q(K)} + |I_p(u - \pi)|_{H^q(K)} \\ &\lesssim h^{s+1-q} |u|_{H^{s+1}(B_K)} + h^{p+1-q} \|\pi\|_{H^{p+1}(K)} + h^{-q+d/2} \|u - \pi\|_{L^\infty(K)} \\ &\lesssim h^{s+1-q} |u|_{H^{s+1}(B_K)} + h^{s+1-q} \|\pi\|_{H^s(B_K)} \lesssim h^{s+1-q} \|u\|_{H^{s+1}(B_K)}, \end{aligned}$$

where in the last estimate we have used the approximation property (10) and the fact that $h \lesssim 1$ (by the boundedness of Ω). Now the desired estimate (9) follows by summing over all elements $K \in \mathcal{T}$ and using the bound (5). ∎

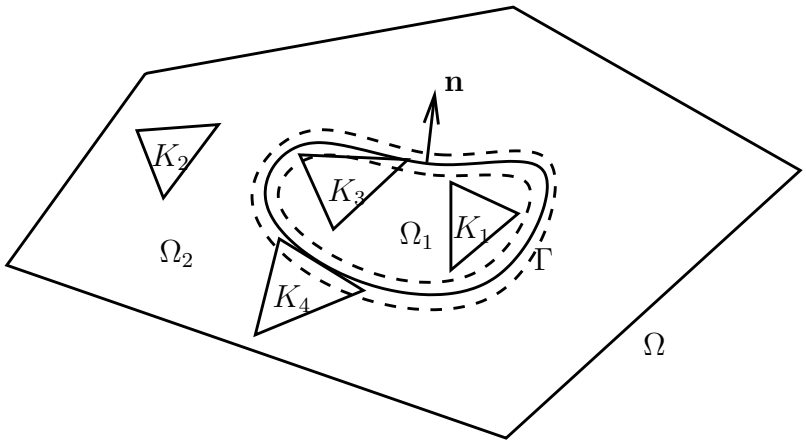

Figure 2: S_δ: region between the two closed dashed lines of width δ around the interface Γ; Interface elements: $K_3 \in \mathcal{T}_*^1$, $K_4 \in \mathcal{T}_*^2$; Non-interface elements: $K_1 \in \mathcal{T}^1$, $K_2 \in \mathcal{T}^2$.

3 A piecewise polynomial interpolation operator

In this section, we study the approximation of piecewise smooth functions by the finite element space $S^{p,1}(\mathcal{T})$. Clearly the accuracy of this approximation depends on how well the mesh $\mathcal{T}$ can resolve the interface Γ. In order to be able to quantify this, we introduce, for $\delta > 0$, the following three neighborhoods of the interface Γ:

$$S_\delta := \{x \in \Omega\,;\ \ \mathrm{dist}\,(x,\Gamma) < \delta\}, \quad S_\delta^i := \{x \in \Omega_i\,;\ \ \mathrm{dist}\,(x,\Gamma) < \delta\} \quad \textit{for } i = 1,2.$$

Definition 3.1. *The triangulation $\mathcal{T}$ is said to resolve the interface Γ* up to error *δ if it can be decomposed as $\mathcal{T} = \mathcal{T}^1 \cup \mathcal{T}^2 \cup \mathcal{T}_*^1 \cup \mathcal{T}_*^2$, where*

$$\mathcal{T}^i = \{K \in \mathcal{T}\,;\quad K \subset \Omega_i \setminus S_\delta\}\,, \quad i = 1,2,$$

and the sets $\mathcal{T}_*^i$ have the property that $K \in \mathcal{T}_*^i$ implies $\max\{\mathrm{dist}\,(x, \Gamma \cap K)\ ;\ \ x \in \overline{K} \cap \overline{\Omega_{i'}}\} \le \delta$. *Here, we denote for $i = 1,2$, by i' the dual index i' by $i' = 1$ if $i = 2$ and $i' = 2$ if $i = 1$.*

We write

$$\Omega_{i,h} := \cup\{K\,;\ \ K \in \mathcal{T}^i \cup \mathcal{T}_*^i\}, \qquad \Gamma_h := \partial\Omega_{1,h} \cap \partial\Omega_{2,h} \tag{11}$$

and $\mathcal{T}_* := \mathcal{T}_*^1 \cup \mathcal{T}_*^2$. Any element in $\mathcal{T}_*$ will be called an interface element and any element K in $\mathcal{T}^1$ or $\mathcal{T}^2$ is called a non-interface element. Figure 2 illustrates the S_δ-region and some typical elements in $\mathcal{T}^1$, $\mathcal{T}^2$, $\mathcal{T}_*^1$ and $\mathcal{T}_*^2$, respectively.

Definition 3.1 does not necessarily imply that the decomposition stated there is unique. Uniqueness is given if δ is significantly smaller than h, which is the case of practical interest. A typical example is the interface-aligned triangulation; see [7]:

Example 3.2. Let Γ be of class C^2 and let $\mathcal{T}$ be an *affine* triangulation with the property that for each element K all its $d+1$ nodes are completely contained in either $\bar{\Omega}_1$ or $\bar{\Omega}_2$. Then the triangulation $\mathcal{T}$ resolves the interface Γ up to error $\delta = O(h^2)$.

Next, we introduce a perturbed nodal interpolation operator I. This operator coincides with the standard Lagrange type interpolation operator I_p on any non-interface element in $\mathcal{T}^i$ $(i = 1,2)$ and is an appropriate modification of I_p on interface elements.

Definition 3.3 (Perturbed nodal interpolation operator)**.** *Let $\mathcal{T}$ be a quasi-uniform regular triangulation in the sense of Definition 2.1 with mesh size h, and let $S^{p,1}(\mathcal{T})$ be the space defined in (6). The operator $I : C(\overline{\Omega}) \to S^{p,1}(\mathcal{T})$ is defined by specifying its nodal values in $\Xi(\mathcal{T})$ as follows:*

1. *For $\xi \in \Xi(\mathcal{T}) \setminus \overline{S_\delta}$, set $(Iu)(\xi) := u(\xi)$;*
2. *For $\xi \in \Xi(\mathcal{T}) \cap \overline{S_\delta}$, choose a point $\widetilde{\xi} \in \Gamma \cap B_{2\delta}(\xi)$ and set $(Iu)(\xi) := u(\widetilde{\xi})$.*

By the definition of S_δ, we know that $\Gamma \cap B_{2\delta}(\xi) \neq \emptyset$ so that the *perturbed* nodal interpolation operator I is well-defined.

Before presenting the approximation properties of the perturbed nodal interpolation operator I, we show the following results about the δ-*strip* S_δ:

Lemma 3.4. *For $z \in H^1(\Omega_1 \cup \Omega_2)$, there holds*

$$\|z\|_{L^2(S_\delta)} \lesssim \sqrt{\delta}\|z\|_{H^1(\Omega_1\cup\Omega_2)}, \tag{12}$$

while for $z \in H^1(\Omega)$ with $z|_\Gamma = 0$ there holds

$$\|z\|_{L^2(S_\delta)} \lesssim \delta\|z\|_{H^1(\Omega)}. \tag{13}$$

Proof. Let us first assume that the function z_i belongs to $C^1(\bar{\Omega}_i)$. For simplicity, we restrict our discussion for the 2D case. But the same ideas of local coordinate systems and the compactness argument can be easily extended to the 3D case.

Since the interface Γ is of C^2-smooth at least, for any fixed point $x \in \Gamma$, let there be $\epsilon > 0$ and $\delta > 0$ to be chosen later, we can define a mapping $F : (-\epsilon, \epsilon) \times (0, \delta) \mapsto \mathbb{R}^2$ as follows

$$F(t, s) = \gamma(t) + s\nu(t).$$

where $\gamma(t) \in \mathbb{R}^2$ is a local representation of the interface curve parametrized by its arc length with $\gamma(0) = x$, and $\nu(t) \in \mathbb{R}^2$ is the unit normal vector of the curve at x pointing inwards Ω_i. A simple calculation gives

$$\frac{\partial F}{\partial s} = \nu(t), \quad \frac{\partial F}{\partial t} = (1 + s\kappa(t))\tau(t).$$

where $\tau(t) \in \mathbb{R}^2$ is the tangential vector of the curve at x and thus

$$\left|\frac{\partial F(t,s)}{\partial(t,s)}\right| = \left|(1 + s\kappa(t)) \det\left(\begin{vmatrix}\tau^T(t)\\ \nu^T(t)\end{vmatrix}\right)\right| = |1 + s\kappa(t)|.$$

The last equality follows from the facts that $\tau(t)$ and $\nu(t)$ are unit vectors and orthogonal to each other. Noting that the curvature κ of the curve is independent of the coordinate systems and continuous along the curve, while the curve Γ is compact in $\mathbb{R}^2$, hence $|\kappa(t)|$ can be bounded by a positive constant. When δ is chosen sufficiently small, we have $0 < c < |\frac{\partial F(t,s)}{\partial(t,s)}| < C$ and thus define a local differmorphism between the a small slice $N^i_\delta(x, \epsilon)$ of the δ-strip region S^i_δ and a small rectangle region in (t, s) coordinate system as shown in Figure 3.

Hence we have

$$\begin{aligned}
\|z_i\|^2_{L^2(N^i_\delta(x,\epsilon))} &= \int_{t=-\epsilon}^{\epsilon}\int_{s=0}^{\delta} |z_i(t,s)|^2(1 + s\kappa(t))\ \mathrm{d}s\mathrm{d}t \\
&\lesssim \delta\int_{t=-\epsilon}^{\epsilon} \max_{0<s<\delta} |z_i(t,s)|^2\ \mathrm{d}t \\
&\lesssim \delta\int_{t=-\epsilon}^{\epsilon}\int_{s=0}^{\delta} |z_i(t,s)|^2 + |\partial_s z_i(t,s)|^2\ \mathrm{d}s\mathrm{d}t \\
&\lesssim \delta\|z_i\|^2_{H^1(N^i_\delta(x,\epsilon))}.
\end{aligned}$$

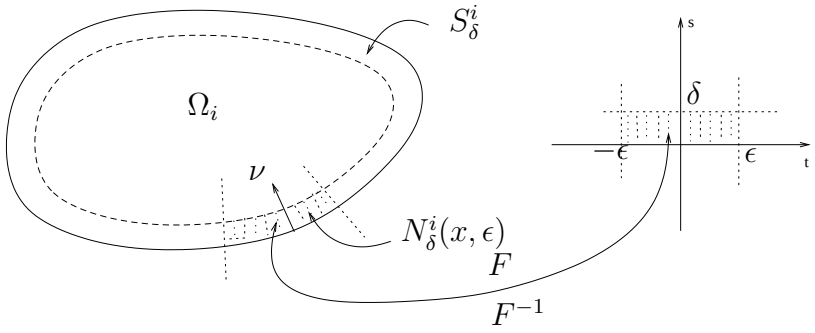

Figure 3: Local coordinate system.

where in the second inequality we make use of the 1D Sobolev embedding $\|u\|_{L^\infty(I)} \lesssim \|u\|_{H^1(I)}$, where $I \subset \mathbb{R}$ is a fixed interval, and in the third inequality we use the facts that $\|\frac{\partial F^{-1}(x,y)}{\partial(x,y)}\| \le C$ and $|\det(\frac{\partial F^{-1}(x,y)}{\partial(x,y)})| \le C$ provided ϵ is chosen small enough.

With the ϵ chosen above fixed, since the interface Γ is compact in $\mathbb{R}^2$, letting the interface be decomposed into a finite number of small curved intervals and applying the *flattening* argument for each interval, we obtain

$$\|z_i\|^2_{L^2(S_\delta^i)} \lesssim \delta \|z_i\|^2_{H^1(S_\delta^i)} \lesssim \delta \|z_i\|^2_{H^1(\Omega_i)}.$$

The desired estimates for $z \in H^1(\Omega_1 \cup \Omega_2)$ follow by taking summation over $i = 1, 2$.

Finally, the second bound basically follows the same lines except using a 1D-Sobolev embedding theorem by observing that $z(t,0) = 0$ implies $|z(t,s)| = |\int_0^s z'(t,x)\,dx| \le C\delta \|z'(t,\cdot)\|_{L^\infty(I)}$ for every $s \in [0,\delta]$. □

Armed with the technical δ-region argument Lemma 3.4, we can now show some approximation properties of the perturbed nodal interpolation operator I.

Theorem 3.5. *Let $d \in \{2,3\}$, let I be the perturbed nodal interpolation introduced in Definition 3.3. Assume that the nodal interpolation operator I_p satisfies Assumption 2.3. Let $s \in \{1,\dots,p\}$ and $\delta \lesssim h$. Then for $u \in H^1(\Omega) \cap H^{s+1}(\Omega_1 \cup \Omega_2)$ there holds for $q \in \{0,1\}$*

$$\|u - Iu\|_{H^q(\Omega)} \lesssim \left(\delta^{1-q/2} + \sqrt{\delta} h^{1-q}\right) \|u\|_{H^2(\Omega_1\cup\Omega_2)} + h^{s+1-q} \|u\|_{H^{s+1}(\Omega_1\cup\Omega_2)}.$$

These estimates can be improved if $s \ge 2$:

$$\begin{aligned}
\|u - Iu\|_{H^q(S_\delta)} &\lesssim \delta^{1-q/2} \|u\|_{H^2(\Omega_1\cup\Omega_2)} + \delta h^{1/2-q} \|u\|_{H^3(\Omega_1\cup\Omega_2)} + h^{s+1-q} \|u\|_{H^{s+1}(\Omega_1\cup\Omega_2)}, \\
\|u - Iu\|_{H^q(\Omega\setminus S_\delta)} &\lesssim \delta h^{1/2-q} \|u\|_{H^3(\Omega_1\cup\Omega_2)} + h^{s+1-q} \|u\|_{H^{s+1}(\Omega_1\cup\Omega_2)}.
\end{aligned}$$

Proof. Noting the fact that the interpolation operators I and I_p coincide on a non-interface element $K \in \mathcal{T}^i$, $i \in \{1,2\}$, Lemma 2.5 gives for $q \in \{0,1\}$ and $i \in \{1,2\}$:

$$\sum_{K\in\mathcal{T}^i} \|u - Iu\|^2_{H^q(K)} \lesssim h^{2(s+1-q)} \|u\|^2_{H^{s+1}(\Omega_i)}.$$

It remains to estimate $\sum_{K\in\mathcal{T}_*^i} \|u - Iu\|^2_{H^q(K)}$. We therefore focus on $\|u - Iu\|_{H^q(K)}$ for an element $K \in \mathcal{T}_*^i$. This is achieved in four steps. Before proceding with further estimates, we recall that $K \in \mathcal{T}_*^i$ implies $K \cap \Omega_{i'} \subset S_\delta$.

Step 1. We claim that for all nodes $\xi \in \Xi(\mathcal{T}) \cap \overline{K}$, there holds

$$|Iu(\xi) - (E_i u)(\xi)| \lesssim \left(\frac{\delta}{r}\right)^{1/2} r^{1-d/2} \left[\|\nabla E_i u\|_{L^2(B_r(\xi))} + r\,|\nabla E_i u|_{H^1(B_r(\xi))}\right], \tag{14}$$

where $B_r(\xi)$ is a ball of radius $r > 0$. If $\xi \in \Xi(\mathcal{T}) \cap \overline{K} \setminus S_\delta$, we know $Iu(\xi) = (E_i u)(\xi)$. So we only need to consider the case with $\xi \in \Xi(\mathcal{T}) \cap \overline{K} \cap S_\delta$. Then by definition of I, we have $Iu(\xi) = u(\widetilde{\xi}) = E_i u(\widetilde{\xi})$ for some $\widetilde{\xi} \in \Gamma \cap B_{2\delta}(\xi)$. For a ball $B_1 \subset \mathbb{R}^d$ $(d = 2, 3)$ of radius 1, the Sobolev embedding $H^2(B_1) \subset C^{0,1/2}(\overline{B}_1)$ (see [1, Chapter 4]) gives for every $v \in H^2(B_1)$ that

$$|v(x) - v(y)| \lesssim |x - y|^{1/2} \left[\|\nabla v\|_{L^2(B_1)} + |\nabla v|_{H^1(B_1)}\right] \qquad \forall\, x, y \in B_1. \tag{15}$$

A scaling argument then yields (14).

Step 2. It follows from Step 1 that

$$\begin{aligned} h^{-1}\|Iu - I_p E_i u\|_{L^2(K)} + \|\nabla(Iu - I_p E_i u)\|_{L^2(K)} &\lesssim h^{d/2-1} \sum_{\xi \in \Xi(\mathcal{T}) \cap \overline{K}} |Iu(\xi) - E_i u(\xi)| \\ &\lesssim \left(\frac{\delta}{r}\right)^{1/2} \left(\frac{r}{h}\right)^{1-d/2} \left[\|\nabla E_i u\|_{L^2(B_r(K))} + r\,|\nabla E_i u|_{H^1(B_r(K))}\right], \end{aligned} \tag{16}$$

where $B_r(K) = \cup_{x \in K} B_r(x)$. We will use $r \sim h$ below.

Step 3. For each $K \in \mathcal{T}_*^i$, we can write

$$(u - Iu)|_K = (u - E_i u)|_K + (E_i u - I_p E_i u)|_K + (I_p E_i u - Iu)|_K\,. \tag{17}$$

Noting that $E_i u = u$ in $K \setminus S_\delta$, we derive for $q = 0, 1$ that

$$\sum_{K \in \mathcal{T}_*^i} \|u - Iu\|^2_{H^q(K \setminus S_\delta)} \lesssim \sum_{K \in \mathcal{T}_*^i} \|E_i u - I_p E_i u\|^2_{H^q(K)} + \sum_{K \in \mathcal{T}_*^i} \|I_p E_i u - Iu\|^2_{H^q(K)}, \tag{18}$$

$$\begin{aligned} \sum_{K \in \mathcal{T}_*^i} \|u - Iu\|^2_{H^q(K \cap S_\delta)} \lesssim{}& \sum_{K \in \mathcal{T}_*^i} \|u - E_i u\|^2_{H^q(K \cap S_\delta)} + \sum_{K \in \mathcal{T}_*^i} \|E_i u - I_p E_i u\|^2_{H^q(K)} \\ &+ \sum_{K \in \mathcal{T}_*^i} \|I_p E_i u - Iu\|^2_{H^q(K)}\,. \end{aligned} \tag{19}$$

By applying Lemma 3.4, we obtain for $q = 0, 1$ that

$$\sum_{K \in \mathcal{T}_*^i} \|u - E_i u\|^2_{H^q(K \cap S_\delta)} \lesssim \sum_{i=1}^{2} \|u - E_i u\|^2_{H^q(S_\delta)} \lesssim \delta^{2-q} \sum_{i=1}^{2} \|u\|^2_{H^2(\Omega_i)}. \tag{20}$$

The smoothness of $E_i u$ implies with Lemma 2.5 that

$$\sum_{K \in \mathcal{T}_*^i} \|E_i u - I_p E_i u\|^2_{H^q(K)} \lesssim h^{2(s+1-q)} \|E_i u\|^2_{H^{s+1}(\Omega_i)} \lesssim h^{2(s+1-q)} \|u\|^2_{H^{s+1}(\Omega_i)}. \tag{21}$$

To bound the terms involving $I_p E_i u - Iu$ in (18) and (19), we wish to employ the estimate (16) with $r \sim h$. To that end, we note that simple geometric considerations gives us

$$\cup_{K \in \mathcal{T}_*} B_h(K) \subset S_{\mu h}$$

for a suitable $\mu > 0$, and the γ-shape regularity of the triangulation implies the existence of $M > 0$ independent of h such that

$$\sup_{x \in S_{\mu h}} \operatorname{card}\{K \in \mathcal{T}_* ;\ x \in B_h(K)\} = M < \infty. \tag{22}$$

Hence, using (16) with $r \sim h$ leads to

$$\sum_{K \in \mathcal{T}_*^i} h^{-2}\|I_p E_i u - Iu\|^2_{L^2(K)} + \|\nabla(I_p E_i u - Iu)\|^2_{L^2(K)} \lesssim M \frac{\delta}{h}\left[\|\nabla E_i u\|^2_{L^2(S_{\mu h})} + h^2 \|\nabla E_i u\|^2_{H^1(S_{\mu h})}\right].$$

Since Lemma 3.4 implies $\|\nabla E_i u\|_{L^2(S_{\mu h})} \lesssim \sqrt{h}\|E_i u\|_{H^2(\Omega_1 \cup \Omega_2)} \lesssim \sqrt{h}\|u\|_{H^2(\Omega_i)}$ we obtain

$$\sum_{K \in \mathcal{T}_*^i} h^{-2}\|I_p E_i u - Iu\|^2_{L^2(K)} + \|\nabla(I_p E_i u - Iu)\|^2_{L^2(K)} \lesssim \delta \|u\|^2_{H^2(\Omega_i)}. \tag{23}$$

Inserting the estimates (20)–(23) in (18)–(19) gives

$$\begin{aligned}
\sum_{K \in \mathcal{T}_*^i} \|u - Iu\|^2_{H^q(K \setminus S_\delta)} &\lesssim \delta h^{2-2q}\|u\|^2_{H^2(\Omega_1 \cup \Omega_2)} + h^{2(p+1-q)}\|u\|^2_{H^{p+1}(\Omega_1 \cup \Omega_2)}, \\
\sum_{K \in \mathcal{T}_*^i} \|u - Iu\|^2_{H^q(K \cap S_\delta)} &\lesssim \delta^{2-q}\|u\|^2_{H^2(\Omega_1 \cup \Omega_2)} + \delta h^{2-2q}\|u\|^2_{H^2(\Omega_1 \cup \Omega_2)} + h^{2(p+1-q)}\|u\|^2_{H^{p+1}(\Omega_1 \cup \Omega_2)}.
\end{aligned}$$

Step 4. We now improve the estimates for the case $s \geq 2$. To that end, we need to modify the argument of Step 1. For $B_1 \subset \mathbb{R}^d$, we have the Sobolev embedding result $H^3(B_1) \subset C^{0,1}(B_1)$, which implies

$$|v(x) - v(y)| \lesssim |x - y| \|\nabla v\|_{H^2(B_1)} \qquad \forall\, v \in H^3(B_1).$$

A scaling argument then produces

$$|Iu(\xi) - E_i u(\xi)| \lesssim \frac{\delta}{r} r^{1-d/2}\left[\|\nabla E_i u\|_{L^2(B_r(\xi))} + r\,|\nabla E_i u|_{H^1(B_r(\xi))} + r^2\,|\nabla E_i u|_{H^2(B_r(\xi))}\right].$$

Now choosing $r \sim h$ and proceeding as we did in Steps 2 and 3 yield

$$\begin{aligned}
&\sum_{K \in \mathcal{T}_*^i} h^{-2}\|I_p E_i u - Iu\|^2_{L^2(K)} + \|\nabla(I_p E_i u - Iu)\|^2_{L^2(K)} \\
&\lesssim \delta^2\left[\frac{1}{h}\|u\|^2_{H^2(\Omega_1 \cup \Omega_2)} + \|u\|^2_{H^2(\Omega_1 \cup \Omega_2)} + h^2\|u\|^2_{H^3(\Omega_1 \cup \Omega_2)}\right] \\
&\lesssim \frac{\delta^2}{h}\|u\|^2_{H^2(\Omega_1 \cup \Omega_2)} + \delta^2 h^2 \|u\|_{H^3(\Omega_1 \cup \Omega_2)} \\
&\lesssim \delta^2 h^{-1}\|u\|^2_{H^3(\Omega_1 \cup \Omega_2)}.
\end{aligned} \tag{24}$$

By inserting the estimates (20)–(21), and the new bound (24) in (18)–(19) we obtain

$$\begin{aligned}
\sum_{K \in \mathcal{T}_*^i} \|u - Iu\|^2_{H^q(K \setminus S_\delta)} &\lesssim \delta^2 h^{1-2q}\|u\|^2_{H^3(\Omega_1 \cup \Omega_2)} + h^{2(s+1-q)}\|u\|^2_{H^{s+1}(\Omega_1 \cup \Omega_2)}, \\
\sum_{K \in \mathcal{T}_*^i} \|u - Iu\|^2_{H^q(K \cap S_\delta)} &\lesssim \delta^{2-q}\|u\|^2_{H^2(\Omega_1 \cup \Omega_2)} + \delta^2 h^{1-2q}\|u\|^2_{H^3(\Omega_1 \cup \Omega_2)} + h^{2(s+1-q)}\|u\|^2_{H^{s+1}(\Omega_1 \cup \Omega_2)}.
\end{aligned}$$

This completes the proof of Theorem 3.5. □

4 Convergence analysis of finite element methods

In this section we formulate the finite element approximation of the interface problem (1)–(3) and establish *a priori* error estimates.

4.1 Formulation of finite element approximation

By integration by parts one can immediately derive the following weak formulation of the interface problem (1)–(3):

Problem (P). Find $u \in H_0^1(\Omega)$ such that

$$a(u,v) = L(v) \quad \forall\ v \in H_0^1(\Omega), \tag{25}$$

where the bilinear form $a(\cdot,\cdot) : H_0^1(\Omega) \times H_0^1(\Omega) \to \mathbb{R}$ is defined by

$$a(u,v) = \sum_{i=1}^{2} \int_{\Omega_i} \beta_i \nabla u_i \cdot \nabla v_i \ \mathrm{d}x, \tag{26}$$

and the linear form $L(v) : H_0^1(\Omega) \to \mathbb{R}$ by

$$L(v) = \sum_{k=1}^{2} \int_{\Omega_i} f v_i \ \mathtt{d}x + \int_{\Gamma} g v \ \mathtt{d}s. \tag{27}$$

The *conforming* finite element discretization of the variational problem (P) then reads:

Problem (P_h^c). Find $u_h \in S_0^{p,1}(\mathcal{T})$ such that

$$a(u_h, v_h) = L(v_h) \quad \forall\ v_h \in S_0^{p,1}(\mathcal{T}). \tag{28}$$

We note that the evaluation of the entries of the stiffness matrix involving interface elements is numerically challenging (especially in 3D) if the mesh is not aligned with the interface. A much more convenient formulation is obtained by using the following approximate bilinear form $a_h(\cdot,\cdot)$:

$$a_h(u,v) = \sum_{K \in \mathcal{T}} \int_K \beta_K \nabla u \cdot \nabla v \, dx, \tag{29}$$

where the coefficients β_K are elementwise smooth. In our present setting of piecewise constant coefficient β, for every $K \in \mathcal{T}$ we take $\beta_K = \beta_i$ if $K \in \mathcal{T}^i \cup \mathcal{T}_*^i$ with $i \in \{1,2\}$. It is immediate to see that the bilinear form $a_h(\cdot,\cdot)$ still preserves the coercivity, and that the two bilinear forms a_h and a are related to each other by

$$a(u,v) = a_h(u,v) + a^{\Delta}(u,v), \tag{30}$$

where the bilinear form $a^{\Delta}(\cdot,\cdot)$ satisfies

$$|a^{\Delta}(u,v)| \lesssim \|u\|_{H^1(S_\delta)} \|v\|_{H^1(S_\delta)}. \tag{31}$$

With the simplified bilinear form in (29), we can now define a more practical finite element method for the variational problem (P).

Problem (P_h). Find $u_h \in S_0^{p,1}(\mathcal{T})$ such that

$$a_h(u_h, v) = L(v) \qquad \forall\, v \in S_0^{p,1}(\mathcal{T}). \tag{32}$$

4.2 General convergence results

We start with a technical lemma to be used in the subsequent convergence analysis.

Lemma 4.1. *For $\delta \lesssim h$, there exists a positive constant μ independent of h such that*

$$\|w_h\|_{H^1(S_\delta)} \lesssim \sqrt{\frac{\delta}{h}} \|w_h\|_{H^1(S_{\mu h})} \quad \forall\, w_h \in S^{p,1}(\mathcal{T}).$$

Proof. The smoothness of the interface Γ and the shape regularity of the triangulation imply that $\mathrm{meas}(K \cap S_\delta) \lesssim h^{d-1}\delta$ for every $K \in \mathcal{T}$. Hence

$$\begin{aligned} \|w_h\|^2_{H^1(S_\delta)} &\leq \sum_{K\in\mathcal{T}: K\cap S_\delta \neq \emptyset} \|w_h\|^2_{H^1(K\cap S_\delta)} \lesssim \sum_{K\in\mathcal{T}: K\cap S_\delta \neq \emptyset} \delta h^{d-1} \|w_h\|^2_{W^{1,\infty}(K)} \\ &\lesssim \sum_{K\in\mathcal{T}: K\cap S_\delta \neq \emptyset} \delta h^{d-1} h^{-d} \|w_h\|^2_{H^1(K)} \lesssim \frac{\delta}{h} \|w_h\|^2_{H^1(S_{\mu h})}, \end{aligned}$$

where we have exploited the assumption $\delta \lesssim h$ in the last estimate. □

We are now ready to derive the H^1- and L^2-norm error estimates.

Theorem 4.2. *Let u and u_h be the solutions to the systems (25) and (32) respectively. Assume that $u \in H^1_0(\Omega) \cap H^{s+1}(\Omega_1 \cup \Omega_2)$ for some $s \in \{1, \ldots, p\}$. Then for $\delta \lesssim h$ the following estimate holds:*

$$\|u - u_h\|_{H^1(\Omega)} \lesssim \sqrt{\delta} \|u\|_{H^2(\Omega_1\cup\Omega_2)} + h^s \|u\|_{H^{s+1}(\Omega_1\cup\Omega_2)}\,.$$

Proof. An application of the first Strang Lemma (see, e.g., [9, Thm. 4.1.1]) to (25) and (32) gives

$$\|u - u_h\|_{H^1(\Omega)} \lesssim \inf_{w\in S^{p,1}_0(\mathcal{T})} \Big\{ \|u - w\|_{H^1(\Omega)} + \sup_{v\in S^{p,1}_0(\mathcal{T})} \frac{|a(w,v) - a_h(w,v)|}{\|v\|_{H^1(\Omega)}} \Big\}. \tag{33}$$

From Theorem 3.5 we have

$$\|u - Iu\|_{H^1(\Omega)} \lesssim h^s \|u\|_{H^{s+1}(\Omega_1\cup\Omega_2)} + \sqrt{\delta} \|u\|_{H^2(\Omega_1\cup\Omega_2)}\,. \tag{34}$$

Next, for all $v \in S^{p,1}(\mathcal{T})$ one can derive by using Lemmas 3.4 and 4.1 that

$$\begin{aligned} |a^\Delta(Iu, v)| &\lesssim \|Iu\|_{H^1(S_\delta)} \|v\|_{H^1(S_\delta)} \lesssim \big(\|u\|_{H^1(S_\delta)} + \|u - Iu\|_{H^1(S_\delta)} \big) \sqrt{\delta} h^{-1/2} \|v\|_{H^1(S_{\mu h})} \\ &\lesssim (\sqrt{\delta} \|u\|_{H^2(\Omega_1\cup\Omega_2)} + h^s \|u\|_{H^{s+1}(\Omega_1\cup\Omega_2)}) \sqrt{\delta} h^{-1/2} \|v\|_{H^1(S_{\mu h})}\,, \end{aligned}$$

which implies with $\delta \lesssim h$ that

$$\sup_{v\in S^{p,1}(\mathcal{T})} \frac{|a^\Delta(Iu, v)|}{\|v\|_{H^1(\Omega)}} \lesssim \sqrt{\delta} \|u\|_{H^2(\Omega_1\cup\Omega_2)} + h^s \|u\|_{H^{s+1}(\Omega_1\cup\Omega_2)}\,. \tag{35}$$

Now the desired estimate follows from (33)–(35). □

Remark 4.3. Theorem 4.2 quantifies the effect of approximating the interface. In order to achieve the optimal p-th order approximation with the finite element space $S^{p,1}(\mathcal{T})$ in H^1-norm, δ must be of the order $O(h^{2p})$.

The L^2-norm estimates for $u - u_h$ can be obtained as usual by duality arguments. We formulate the necessary shift theorem for the appropriate dual problem as an assumption:

Assumption 4.4 (full dual regularity)**.** *For $g = 0$ and every $f \in L^2(\Omega)$ the solution u of (1)–(3) satisfies $u \in H_0^1(\Omega) \cap H^2(\Omega_1 \cup \Omega_2)$ together with the a priori estimate $\|u\|_{H^2(\Omega_1 \cup \Omega_2)} \leq C\|f\|_{L^2(\Omega)}$.*

Remark 4.5. Assumption 4.4 is satisfied if Ω is convex or $\partial\Omega$ is sufficiently smooth, [7, 21].

Theorem 4.6 below gives error estimates for the L^2-error of the FEM. Surprisingly, the conditions on the degree of approximation of the interface to obtain the optimal convergence are not as strong as those for optimal convergence in H^1-norm. In particular, for $p > 1$, isoparametric elements lead to optimal rates in L^2 but not in H^1. For example, isoparametric quadratic finite elements achieve optimal third order convergence in the L^2-norm but only order 1.5 in the energy norm in general.

Theorem 4.6. *Under the hypotheses of Theorem 4.2 and Assumption 4.4, the following estimate holds:*

$$\|u - u_h\|_{L^2(\Omega)} \lesssim (h^{s+1} + \delta)\|u\|_{H^{s+1}(\Omega_1 \cup \Omega_2)}. \tag{36}$$

Proof. Abbreviate $e := u - u_h$. By Theorem 4.2 we have

$$\|e\|_{H^1(\Omega)} \lesssim h^s \|u\|_{H^{s+1}(\Omega_1 \cup \Omega_2)} + \sqrt{\delta}\|u\|_{H^2(\Omega_1 \cup \Omega_2)}. \tag{37}$$

For the duality argument, we define $w \in H_0^1(\Omega)$ and $w_h \in S_0^{p,1}(\mathcal{T})$ by

$$a(v, w) = (u - u_h, v)_{L^2(\Omega)} \qquad \forall v \in H_0^1(\Omega), \tag{38}$$

$$a(v, w_h) = (u - u_h, v)_{L^2(\Omega)} \qquad \forall v \in S_0^{p,1}(\mathcal{T}). \tag{39}$$

That is, w is the weak solution to the interface problem (1)–(3) with $g = 0$. Assumption 4.4 implies $w \in H^2(\Omega_1 \cup \Omega_2)$ with the *a priori* bound

$$\|w\|_{H^2(\Omega_1 \cup \Omega_2)} \lesssim \|u - u_h\|_{L^2(\Omega)}. \tag{40}$$

The function $w_h \in S_0^{p,1}(\mathcal{T})$ is the Galerkin approximation of w. Céa's Lemma together with Theorem 3.5 therefore gives

$$\begin{aligned} \|w - w_h\|_{H^1(\Omega)} &\lesssim \inf_{v \in S_0^{p,1}(\mathcal{T})} \|w - v\|_{H^1(\Omega)} \leq \|w - Iw\|_{H^1(\Omega)} \\ &\lesssim (h + \sqrt{\delta})\|w\|_{H^2(\Omega_1 \cup \Omega_2)} \lesssim (h + \sqrt{\delta})\|u - u_h\|_{L^2(\Omega)}. \end{aligned} \tag{41}$$

It is easy to verify the following Galerkin orthogonalities for $u - u_h$ and $w - w_h$:

$$\begin{aligned} a(e, v) &= -a^{\Delta}(u_h, v) \qquad \forall v \in S_0^{p,1}(\mathcal{T}), \\ a(v, w - w_h) &= 0 \qquad \forall v \in S_0^{p,1}(\mathcal{T}). \end{aligned}$$

These two Galerkin orthogonalities imply that

$$\|e\|_{L^2(\Omega)}^2 = a(e, w) = a(e, w - w_h) + a(e, w_h) = a(u - Iu, w - w_h) - a^{\Delta}(u_h, w_h).$$

Recognizing the bilinear form a as an integral over Ω that can be split into integrals over S_δ and $\Omega \setminus S_\delta$, we obtain with the estimate (31) that

$$\begin{aligned}\|e\|^2_{L^2(\Omega)} &\lesssim \|u-Iu\|_{H^1(S_\delta)}\|w-w_h\|_{H^1(S_\delta)} + \|u-Iu\|_{H^1(\Omega\setminus S_\delta)}\|w-w_h\|_{H^1(\Omega\setminus S_\delta)} \\ &\quad + \|u_h\|_{H^1(S_\delta)}\|w_h\|_{H^1(S_\delta)} =: T_1+T_2+T_3. \end{aligned} \tag{42}$$

We now claim

$$\|u_h\|_{H^1(S_\delta)} \lesssim (h^s+\sqrt{\delta})\|u\|_{H^{s+1}(\Omega_1\cup\Omega_2)}\,, \tag{43}$$

$$\|w\|_{H^1(S_\delta)} + \|w_h\|_{H^1(S_\delta)} \lesssim \sqrt{\delta}\|e\|_{L^2(\Omega)}. \tag{44}$$

To see (43), we apply Lemma 3.4 to obtain

$$\|u_h\|_{H^1(S_\delta)} \le \|e\|_{H^1(S_\delta)} + \|u\|_{H^1(S_\delta)} \lesssim \|e\|_{H^1(\Omega)} + \sqrt{\delta}\|u\|_{H^2(\Omega_1\cup\Omega_2)}.$$

Then the error bound (37) leads immediately to (43). The bound $\|w\|_{H^1(S_\delta)} \lesssim \sqrt{\delta}\|e\|_{L^2(\Omega)}$ follows from Lemma 3.4 and the regularity assertion (40). For the bound of $\|w_h\|_{H^1(S_\delta)}$, we use Lemma 4.1, the estimate (41), and the regularity assertion (40) to get

$$\begin{aligned}\|w_h\|_{H^1(S_\delta)} &\lesssim \sqrt{\delta}h^{-1/2}\|w_h\|_{H^1(S_{\mu h})} \lesssim \sqrt{\delta}h^{-1/2}\left(\|w-w_h\|_{H^1(S_{\mu h})} + \|w\|_{H^1(S_{\mu h})}\right) \\ &\lesssim \sqrt{\delta}h^{-1/2}\left(\|w-w_h\|_{H^1(S_{\mu h})} + h^{1/2}\|w\|_{H^2(\Omega_1\cup\Omega_2)}\right) \\ &\lesssim \left(\sqrt{\delta h} + \delta h^{-1/2} + \sqrt{\delta}\right)\|e\|_{L^2(\Omega)}, \end{aligned}$$

which yields the estimate (44) in view of $\delta \lesssim h$.

Now we will estimate the three terms T_3, T_2 and T_1 in (42) one by one. First for T_3, it follows from (43) and (44) that

$$T_3 \lesssim \sqrt{\delta}(h^s+\sqrt{\delta})\|u\|_{H^{s+1}(\Omega_1\cup\Omega_2)}\|e\|_{L^2(\Omega)}\,.$$

Then noting that $s \ge 1$ and $h^s\sqrt{\delta} \lesssim h^{2s} + \delta$, we see that T_3 can be bounded in the desired fashion.

For the estimate of T_2 with $s \ge 2$, we obtain by applying Theorem 3.5 and (41) that

$$\begin{aligned} T_2 &\lesssim \left(\delta h^{-1/2}\|u\|_{H^3(\Omega_1\cup\Omega_2)} + h^s\|u\|_{H^{s+1}(\Omega_1\cup\Omega_2)}\right)(h+\sqrt{\delta})\|e\|_{L^2(\Omega)} \\ &\lesssim \left(\delta h^{1/2} + \delta\sqrt{\delta}h^{-1/2} + h^{s+1} + h^s\sqrt{\delta}\right)\|u\|_{H^{s+1}(\Omega_1\cup\Omega_2)}\|e\|_{L^2(\Omega)} \\ &\lesssim \left(h^{s+1}+\delta\right)\|u\|_{H^{s+1}(\Omega_1\cup\Omega_2)}\|e\|_{L^2(\Omega)}, \end{aligned}$$

since $\delta \lesssim h$ and $h^s\sqrt{\delta} \lesssim h^{2s} + \delta \lesssim h^{s+1} + \delta$. This is an estimate of the desired form. The case with $s = 1$ is completely analogous and therefore omitted.

Finally for T_1, it follows from (44) that

$$\begin{aligned} T_1 &\lesssim \|u-Iu\|_{H^1(\Omega)}\left(\|w\|_{H^1(S_\delta)} + \|w_h\|_{H^1(S_\delta)}\right) \lesssim \left(\sqrt{\delta}+h^s\right)\|u\|_{H^{s+1}(\Omega_1\cup\Omega_2)}\sqrt{\delta}\|e\|_{L^2(\Omega)} \\ &\lesssim \left(\delta + h^s\sqrt{\delta}\right)\|u\|_{H^{s+1}(\Omega_1\cup\Omega_2)}\|e\|_{L^2(\Omega)}. \end{aligned}$$

Again, we arrive at an estimate of the desired form. This completes the proof of Theorem 4.6. □

4.3 Applications and extensions

Theorems 4.2 and 4.6 quantify the convergence behavior of the finite element method in terms of the mesh size h and the parameter δ, which measures how well the triangulation resolves the interface Γ. An important case of finite elements is that of *polynomial* element maps of degree $m \in \mathbb{N}$. The use of polynomial element maps results in a piecewise polynomial approximation of Γ; hence, one expects $\delta = O(h^{m+1})$. We recall a standard terminology: the case $m < p$ is referred to as *subparametric elements*, the case $m = p$ as *isoparametric elements* and the case $m > p$ as *superparametric elements*; see [5, 9]. The construction of the element maps F_K was studied systematically in [16] in a way that not only Assumption 2.3 but also the approximation order of the interface $\delta = O(h^{m+1})$ are satisfied. Following [16, Lemma 5], one can show

Lemma 4.7. *Let the interface Γ be of of class C^{m+1} and let $\mathcal{T}$ be a triangulation of Ω satisfying Definition 2.1, with all its element maps F_K defined by the m-th order polynomials in a practical manner (see [16] for details). Then the triangulation $\mathcal{T}$ resolves the interface Γ up to the error $\delta = O(h^{m+1})$.*

Lemma 4.7, along with Theorems 4.2 and 4.6, implies immediately the following convergence results:

Theorem 4.8 (isoparametric and superparametric elements)**.** *Let Γ be sufficiently smooth and the element maps F_K be polynomials of degree m as constructed in [16]. Let u and u_h be the solutions to the systems (25) and (32), with u satisfying that $u \in H^{p+1}(\Omega_1 \cup \Omega_2)$. Then:*

1. *For* isoparametric *elements with $m = p$, there holds*

$$\|u - u_h\|_{H^1(\Omega)} \lesssim h^{(p+1)/2} \|u\|_{H^{p+1}(\Omega_1 \cup \Omega_2)}.$$

2. *For* superparametric *elements with $m \geq 2p - 1$, there holds*

$$\|u - u_h\|_{H^1(\Omega)} \lesssim h^{p} \|u\|_{H^{p+1}(\Omega_1 \cup \Omega_2)}.$$

If Assumption 4.4 holds, then there holds in both cases additionally

$$\|u - u_h\|_{L^2(\Omega)} \lesssim h^{p+1} \|u\|_{H^{p+1}(\Omega_1 \cup \Omega_2)}.$$

Remark 4.9. Theorem 4.8 reveals that linear finite elements ($m = p = 1$) indeed achieve optimal convergence order both in the H^1- and L^2-norms. While for higher order finite elements, isoparametric finite elements yields optimal convergence in the L^2-norm, but not in the H^1-norm. One has to resort to superparametric finite elements to recover the optimal convergence for the H^1-norm.

For the sake of exposition and clarity, we have chosen to avoid a few rather technical but practically important issues in the current work. Nevertheless, we believe that the theory of the present paper can be generalized in the following directions:

- *Piecewise smooth coefficients:* We have restricted our attention to piecewise constant coefficients β in (1). However, all our results can be extended to piecewise smooth coefficients. In this case, one just needs to replace the constant β_K in (29) by some appropriate approximation of $\beta|_K$, e.g, an average or an interpolant of β.

- *Quasi-uniform triangulations:* The convergence theory has been established for quasi-uniform meshes. Conceivably, the analysis can be extended to more general, shape-regular triangulations with local mesh refinement. The assumption of quasi-uniformity, which is reasonable in the case of piecewise smooth solutions considered here, allows us to simplify covering arguments in the estimates (5) and (22).
- *Elasticity problems:* Using the vector-valued forms of the finite element spaces discussed in this work, one can solve elastic interface problems as well. Vectorized versions of the perturbed interpolation operator of Definition 3.3, the δ-region argument of Lemma 3.4, and the approximation property of Theorem 3.5 can be derived analogously without essential modifications. In particular, for the simplest case with continuous piecewise linear finite elements with $p = m = 1$, vectorized version of Theorem 4.8 can be derived in a similar way. Optimal convergence, e.g. first order in energy norm and second order in L^2-norm, can readily be derived for the Lamé system.
- *Treatment of non-homogeneous interface source functions g:* In our analysis, we have ignored variational crimes stemming from approximating the right-hand side $L(\cdot)$, which arises in particular when $g \neq 0$. In this situation, a numerically feasible realization of $L(\cdot)$ is likely to be based on the approximate interface Γ_h, which is a union of faces of elements. It is likely that the error introduced by the approximation can be quantified with techniques similar to [7] and the present paper provided that Γ_h and Γ are sufficiently close in an appropriate sense.

4.4 Convergence away from the interface

We recall that Theorem 4.8 indicates that isoparametric elements do not achieve optimal convergence rates in the H^1-norm, which is due to the poor approximation within the strip region S_δ around the interface. Indeed, as it will be seen in Theorem 4.14 below, the condition $\delta = O(h^{p+1})$ is sufficient to ensure optimal H^1-norm convergence of order $O(h^p)$ in the region $\Omega \setminus S_\delta$ away from the interface, as long as the exact solution u is sufficiently smooth in $\Omega \setminus S_\delta$.

Our main results of this subsection (Theorem 4.14) are established based on a duality argument. In order to stress the fact that rather weak regularity requirements for the solution to the dual system of the original interface problem (1)–(3) are sufficient for the optimal H^1 convergence in $\Omega \setminus S_\delta$, we formulate the following assumption, which states that for every $f \in L^2(\Omega)$ the solution to the dual problem has Sobolev regularity $H^{3/2}$ near $\partial\Omega$ and is piecewise H^2 near the interface.

Assumption 4.10. *There exist two domains Ω_1' and Ω_2' with $\overline{\Omega_1} \subset \Omega_1' \subset \overline{\Omega_1'} \subset \Omega_2' \subset \overline{\Omega_2'} \subset \Omega$ such that for every $f \in L^2(\Omega)$ the solution u of the elliptic system (1)–(3) with $g = 0$ satisfies $u \in H_0^1(\Omega) \cap H^{3/2}(\Omega \setminus \overline{\Omega_1'}) \cap H^2((\Omega_1 \cup \Omega_2) \cap \Omega_2')$ together with the following a priori estimate:*

$$\|u\|_{H^2((\Omega_1 \cup \Omega_2) \cap \Omega_2')} + \|u\|_{H^{3/2}(\Omega \setminus \overline{\Omega_1'})} \leq C \|f\|_{L^2(\Omega)}. \tag{45}$$

Remark 4.11. Assumption 4.10 is true in the present case of piecewise constant coefficient β for polygonal (2D) or polyhedral (3D) Lipschitz domains: The smoothness of Γ and $f \in L^2(\Omega)$ implies by standard arguments that $u \in H^2((\Omega_1 \cup \Omega_2) \cap \Omega_2')$ (see, e.g., [7]). For the $H^{3/2}$-regularity near $\partial\Omega$, let χ be a smooth cut-off function with $\chi \equiv 1$ on $\Omega \setminus \overline{\Omega_1'}$ and $\chi \equiv 0$ on an open neighborhood of $\overline{\Omega_1}$. The function $\widetilde{u} := \chi u$ then satisfies $-\Delta\widetilde{u} \in L^2(\Omega)$ and coincides with u on $\Omega \setminus \overline{\Omega_1'}$. By [10, Rem. 2.4.6] for the 2D case and by [10, Cor. 2.6.7] for the 3D case there exists $s_0 \in (3/2, 2]$ and $C > 0$ (both depending solely on Ω) such that $\widetilde{u}$ satisfies $\|\widetilde{u}\|_{H^{s_0}(\Omega)} \leq C \|\Delta\widetilde{u}\|_{L^2(\Omega)}$. The argument is concluded by noting $\|\Delta\widetilde{u}\|_{L^2(\Omega)} \leq C \|f\|_{L^2(\Omega)}$.

Now we can derive our first approximation result.

Lemma 4.12. *Assume that Assumption 2.3 holds for I_p and let $s \in [1, p+1]$ be a real number. Then there exists a constant $C > 0$ independent of h such that the following approximation*

$$\inf_{v \in S_0^{p,1}(\mathcal{T})} \|w - v\|_{L^2(\Omega)} + h\|w - v\|_{H^1(\Omega)} \leq Ch^s \|w\|_{H^s(\Omega)}$$

is satisfied for all $w \in H^s(\Omega) \cap H_0^1(\Omega)$.

Proof. Let $w \in H^s(\Omega) \cap H_0^1(\Omega)$. It follows from [5, Thm. 12.4.2] and the approximation properties of I_p that there exists a $v \in S^{p,1}(\mathcal{T})$ such that

$$\|w - v\|_{L^2(\Omega)} + h\|w - v\|_{H^1(\Omega)} \lesssim h^s \|w\|_{H^s(\Omega)}. \tag{46}$$

Since v does not necessarily vanish on $\partial\Omega$, we define the correction $v_c \in S^{p,1}(\mathcal{T})$ by the condition that v_c vanish at all nodes that lie strictly inside Ω and $v_c(V) = -v(V)$ for all nodes V lying on $\partial\Omega$. Then we have $v + v_c \in S_0^{p,1}(\mathcal{T})$. For each node $V \in \partial\Omega$, we set $\Gamma_V := \cup\{\overline{K} \cap \partial\Omega\,;\ V \in \overline{K}\}$. By the shape regularity of the triangulation and the assumption on the element maps, there exist two positive integers M and M' independent of h such that every point $x \in \partial\Omega$ lies in at most M sets Γ_V, and every node $V \in \partial\Omega$ is a node of at most M' elements in $\mathcal{T}$. Finally, for every node $V \in \partial\Omega$ there exists an element $K \in \mathcal{T}$ and a face f (3D) (or an edge (2D)) of K such that $f \subset \partial\Omega$ and $V \in \overline{f}$; hence $f \subset \Gamma_V$. We have by the standard inverse estimate that $|v_c(V)| \lesssim h^{-(d-1)/2} \|v_c\|_{L^2(\Gamma_V)}$. With further inverse estimates for $q \in \{0, 1\}$, we derive

$$\begin{aligned}
\|v_c\|_{H^q(\Omega)}^2 &\leq \sum_{K:\overline{K}\cap\partial\Omega\neq\emptyset} \|v_c\|_{H^q(K)}^2 \lesssim \sum_{K:\overline{K}\cap\partial\Omega\neq\emptyset} \sum_{V:V\in\overline{K}\cap\partial\Omega} h^{d-2q}|v_c(V)|^2 \\
&\lesssim h^{d-2q} \sum_{V\in\partial\Omega} \sum_{K:V\in\overline{K}} |v_c(V)|^2 \leq M' h^{d-2q} \sum_{V\in\partial\Omega} |v_c(V)|^2 \\
&\lesssim h^{d-2q} h^{-(d-1)} \sum_{V:V\in\partial\Omega} \|v_c\|_{L^2(\Gamma_V)}^2 \leq M h^{1-2q} \|v_c\|_{L^2(\partial\Omega)}^2.
\end{aligned}$$

Since $w|_{\partial\Omega} = 0$ and $v_c|_{\partial\Omega} = -v|_{\partial\Omega}$ we can estimate with a multiplicative trace inequality $\|v_c\|_{L^2(\partial\Omega)}^2 = \|w - v\|_{L^2(\partial\Omega)}^2 \lesssim \|w - v\|_{L^2(\Omega)} \|w - v\|_{H^1(\Omega)} \lesssim h^{2s-1} \|w\|_{H^s(\Omega)}^2$. We conclude $\|v_c\|_{H^q(\Omega)} \lesssim h^{1/2-q+s-1/2} \|w\|_{H^s(\Omega)} \lesssim h^{s-q} \|w\|_{H^s(\Omega)}$, which, along with the triangle inequality, indicates that (46) is also true when v is replaced by $v + v_c$, hence proves the desired estimate in Lemma 4.12. □

The next lemma shows an L^2-norm error estimate under weaker assumptions than those of Theorem 4.6. Although the accuracy obtained here is also lower than in Theorem 4.6 (by a half order), it suffices for us to recover the optimal H^1 convergence rate for the isoparametric elements in the region away from the interface (see Theorem 4.14).

Lemma 4.13. *Let u and u_h be the solutions to the systems (25) and (32) respectively, with u satisfying $u \in H_0^1(\Omega) \cap H^{s+1}(\Omega_1 \cup \Omega_2)$ for some $s \in \{2, \ldots, p\}$. Then under Assumption 4.10 the following estimate holds for $\delta \lesssim h$:*

$$\|u - u_h\|_{L^2(\Omega)} \lesssim (\delta + h^{s+1/2}) \|u\|_{H^{s+1}(\Omega_1 \cup \Omega_2)}.$$

Proof. The proof follows the arguments of the proof of Theorem 4.6, taking care, however, of the fact that the solution w to the dual problem

$$-\nabla\cdot(\beta\nabla w) = u - u_h \quad \text{in } \Omega, \qquad w|_{\partial\Omega} = 0,$$

may not be in $H^2(\Omega_1\cup\Omega_2)$ now. By Assumption 4.10 we know that w satisfies

$$\|w\|_{H^2((\Omega_1\cup\Omega_2)\cap\Omega_2')} + \|w\|_{H^{3/2}(\Omega\setminus\overline{\Omega_1'})} \le C\|u-u_h\|_{L^2(\Omega)}.$$

Next, we select a smooth cut-off function χ with $\operatorname{supp}\chi \subset \overline{\Omega\setminus\Omega_1'}$ and $\chi\equiv 1$ on $\Omega\setminus\Omega_2'$, where Ω_1', Ω_2' are given in Assumption 4.10. Then Assumption 4.10 ensures $w\chi\in H^{3/2}(\Omega)\cap H_0^1(\Omega)$ and $w(1-\chi)\in H^2(\Omega_1\cup\Omega_2)\cap H_0^1(\Omega)$. By applying Lemma 4.12 to approximate $w\chi$ and Theorem 3.5 to approximate $w(1-\chi)$, we know the existence of a $\widetilde{w}_h\in S_0^{p,1}(\mathcal{T})$ such that

$$\|w-\widetilde{w}_h\|_{H^1(\Omega)} \lesssim \left(h^{1/2}+\sqrt{\delta}\right)\|u-u_h\|_{L^2(\Omega)}.$$

As in the proof of Theorem 4.6, letting w_h be the finite element approximation of w in $S_0^{p,1}(\mathcal{T})$ produces $\|w-w_h\|_{H^1(\Omega)}\lesssim\|w-\widetilde{w}_h\|_{H^1(\Omega)}$ by Céa's Lemma. Now the desired error estimate follows by repeating the remaining steps of the proof of Theorem 4.6. □

The next theorem demonstrates that the optimal H^1-convergence can be achieved in the region $\Omega\setminus S_\delta$ away from the interface.

Theorem 4.14. *Let u and u_h be the solutions to the systems (25) and (32) respectively, and assume $u\in H_0^1(\Omega)\cap H^{s+1}(\Omega_1\cup\Omega_2)$ for some $s\in\{1,\dots,p\}$. Then under Assumption 4.10 the following estimate holds for $\delta\lesssim h$:*

$$\|u-u_h\|_{H^1(\Omega\setminus S_\delta)} \lesssim \operatorname{err}(s,\delta,h)\|u\|_{H^{s+1}(\Omega_1\cup\Omega_2)}$$

where $\operatorname{err}(s,\delta,h)$ *is given by*

$$\operatorname{err}(s,\delta,h) = \begin{cases} h+\delta^{1/2} & \text{for } s=1 \\ h^s + \left(\frac{\delta}{h}\right)^{3/2} + \left(\frac{\delta}{h}\right)h^{1/4} + \left(\frac{\delta}{h}\right)^{3/4}h^{s/2} + \left(\frac{\delta}{h}\right)^{1/2}h^{s/2} + \left(\frac{\delta}{h}\right)^{1/4}h^{s-1/4} & \text{for } s\ge 2 \end{cases}$$

which leads to the optimal convergence when $\delta = O(h^{s+1})$:

$$\|u-u_h\|_{H^1(\Omega\setminus S_\delta)}\lesssim h^s\|u\|_{H^{s+1}(\Omega_1\cup\Omega_2)}.$$

Proof. The case $s=1$ follows trivially from Theorem 4.2. For the case $s\ge 2$ set $e := u-u_h$ and denote by $a_{h,\Omega\setminus S_\delta}$ and a_{h,S_δ} the bilinear form a_h in (29) when the domain of integration is restricted on $\Omega\setminus S_\delta$ and S_δ respectively. It follows from the Galerkin orthogonality that

$$a_h(e,v) = -a^\Delta(u,v) \qquad \forall v\in S_0^{p,1}(\mathcal{T}).$$

Using this Galerkin orthogonality and the Cauchy-Schwarz inequality we obtain

$$\begin{aligned}
\|e\|_{H^1(\Omega\setminus S_\delta)}^2 &\lesssim a_{h,\Omega\setminus S_\delta}(e,e) = a_h(e,e) - a_{h,S_\delta}(e,e) \\
&= a_h(e,u-Iu) - a^\Delta(e,Iu-u_h) - a_{h,S_\delta}(e,e) \\
&= a_{h,\Omega\setminus S_\delta}(e,u-Iu) - a^\Delta(e,Iu-u_h) - a_{h,S_\delta}(e,Iu-u_h) \\
&\lesssim \|e\|_{H^1(\Omega\setminus S_\delta)}\|u-Iu\|_{H^1(\Omega\setminus S_\delta)} + \|e\|_{H^1(S_\delta)}\|Iu-u_h\|_{H^1(S_\delta)}.
\end{aligned}$$

Then we derive by using the Young's inequality for the first term and the triangle inequality for the second term above that

$$\|e\|^2_{H^1(\Omega\setminus S_\delta)} \lesssim \|u-Iu\|^2_{H^1(\Omega\setminus S_\delta)} + \|Iu-u_h\|^2_{H^1(S_\delta)} + \|u-Iu\|_{H^1(S_\delta)}\|Iu-u_h\|_{H^1(S_\delta)}. \quad (47)$$

For the error $Iu-u_h$ in (47), we can estimate it in S_δ by using Lemmas 4.1 and 4.13 and Theorem 3.5 (with $s\geq 2$) as follows:

$$\begin{aligned} \|Iu-u_h\|_{H^1(S_\delta)} &\lesssim \delta^{1/2}h^{-1/2}\|Iu-u_h\|_{H^1(S_{\mu h})} \lesssim \delta^{1/2}h^{-3/2}\|Iu-u_h\|_{L^2(S_{\mu h})} \\ &\lesssim \delta^{1/2}h^{-3/2}\left(\|Iu-u\|_{L^2(S_{\mu h})} + \|u-u_h\|_{L^2(S_{\mu h})}\right)) \\ &\lesssim \delta^{1/2}h^{-3/2}\left(\delta + h^{s+1/2}\right)\|u\|_{H^{s+1}(\Omega_1\cup\Omega_2)}. \end{aligned} \quad (48)$$

Using this and Theorem 3.5 again we conclude from (47) for $\delta \lesssim h$ that

$$\begin{aligned} &\|e\|^2_{H^1(\Omega\setminus S_\delta)} \\ \lesssim\ & \left\{\delta^2h^{-1} + h^{2s} + \delta h^{-3}(\delta^2+h^{2s+1}) + (\delta^{1/2}+h^s)\delta^{1/2}h^{-3/2}(\delta+h^{s+1/2})\right\}\|u\|^2_{H^{s+1}(\Omega_1\cup\Omega_2)} \\ \lesssim\ & \left\{\delta^2h^{-1} + h^{2s} + \delta^3h^{-3} + \delta h^{2s-2} + \delta^2h^{-3/2} + \delta h^{s-1} + \delta^{3/2}h^{s-3/2} + \delta^{1/2}h^{2s-1}\right\}\|u\|^2_{H^{s+1}(\Omega_1\cup\Omega_2)} \end{aligned}$$

which gives the desired estimate for $s\geq 2$ in Theorem 4.14 by taking the square root on both sides. □

The optimal H^1-convergence of Theorem 4.14 enables us to generalize a result in [3, Thm. 2.1]:

Corollary 4.15. *Let u and u_h be the solutions to the systems (25) and (32) respectively, and assume $u\in H^1_0(\Omega)\cap H^{p+1}(\Omega_1\cup\Omega_2)$. Then under Assumption 4.10 the following estimate holds for $\delta = O(h^{p+1})$:*

$$\sum_{i=1}^2 \|\widetilde{u}_i - u_h\|_{H^1(\Omega_{i,h})} \lesssim h^p\left(\sum_{i=1}^2 \|u\|_{H^{p+1}(\Omega_i)} + \|\widetilde{u}_i\|_{H^{p+1}(\Omega)}\right).$$

where $\Omega_{i,h} := \cup\{K\,;\, K\in\mathcal{T}^i\cup\mathcal{T}^i_*\}$ and $\widetilde{u}_i\in H^{p+1}(\mathbb{R}^d)$ is an extension of the function $u_i = u|_{\Omega_i}$ for $i=1,2$.

Proof. We will make use of some key observations in the following proof: for each $K\in\mathcal{T}$, there exists a fixed (open) ball $\widehat{B}\subset\widehat{K}$ that is independent of h such that $F_K(\widehat{B})\subset K\setminus S_\delta$; this implies that $\widetilde{u}_i|_{F_K(\widehat{B})} = u|_{F_K(\widehat{B})}$ for each $K\in\mathcal{T}^i\cup\mathcal{T}^i_*$; all the norms are equivalent on the finite-dimensional space of polynomials of degree p, namely $\|\pi\|_{H^1(\widehat{K})}\sim\|\pi\|_{H^1(\widehat{B})}$ for all $\pi\in\mathcal{P}_p(\widehat{K})$.

Now for any $K\in\mathcal{T}^i\cup\mathcal{T}^i_*$, we define $\widehat{\widetilde{u}} := \widetilde{u}_i|_K\circ F_K$, $\widehat{u} := u|_K\circ F_K$, $\widehat{u}_h := u_h|_K\circ F_K$. Recalling the operator I_p of Section 2.2 and estimate (8), we derive for $q\in\{0,1\}$ that

$$\begin{aligned} \|\widetilde{u}_i - u_h\|_{H^q(K)} &\leq \|\widetilde{u}_i - I_p\widetilde{u}_i\|_{H^q(K)} + \|I_p\widetilde{u}_i - u_h\|_{H^q(K)} \\ &\lesssim h^{p+1-q}\|\widetilde{u}_i\|_{H^{p+1}(K)} + h^{d/2-q}\|\widehat{I}_p\widehat{\widetilde{u}} - \widehat{u}_h\|_{H^q(\widehat{K})}. \end{aligned}$$

The second term above can be estimated further as follows:

$$\begin{aligned} h^{d/2-q}\|\widehat{I}_p(\widehat{\widetilde{u}}-\widehat{u}_h)\|_{H^q(\widehat{K})} &\lesssim h^{d/2-q}\|\widehat{I}_p(\widehat{\widetilde{u}}-\widehat{u}_h)\|_{H^q(\widehat{B})} \\ &\leq h^{d/2-q}\|\widehat{I}_p\widehat{\widetilde{u}}-\widehat{\widetilde{u}}\|_{H^q(\widehat{B})}+h^{d/2-q}\|\widehat{\widetilde{u}}-\widehat{u}_h\|_{H^q(\widehat{B})} \\ &\lesssim \|I_p\widetilde{u}_i-\widetilde{u}_i\|_{H^q(K)}+\|\widetilde{u}_i-u_h\|_{H^q(K\setminus S_\delta)} \\ &\lesssim \|I_p\widetilde{u}_i-\widetilde{u}_i\|_{H^q(K)}+\|u-u_h\|_{H^q(K\setminus S_\delta)} \\ &\lesssim h^{p+1-q}\|\widetilde{u}_i\|_{H^{p+1}(K)}+\|u-u_h\|_{H^q(K\setminus S_\delta)}. \end{aligned}$$

Now summing up both sides over all elements yields

$$\sum_{i=1}^{2}\sum_{K\in\mathcal{T}^i\cup\mathcal{T}^i_*}\|\widetilde{u}_i-u_h\|^2_{H^q(K)}\lesssim\sum_{i=1}^{2}\sum_{K\in\mathcal{T}^i\cup\mathcal{T}^i_*}h^{2(p+1-q)}\|\widetilde{u}_i\|^2_{H^{p+1}(K)}+\|u-u_h\|^2_{H^q(\Omega\setminus S_\delta)}.$$

This allows us to conclude the proof by an appeal to Theorem 4.14. □

Remark 4.16. One possible choice of the extension $\widetilde{u}_i$ used in Corollary 4.15 is given by the Stein extension $E_iu|_{\Omega_i}$. Corollary 4.15 shows that the finite element approximation u_h is closer to $E_iu|_{\Omega_i}$ on $\Omega_{i,h}$ than to u in the case $\delta = O(h^{p+1})$. This improvement over Theorem 4.8 is achieved by changing the measurement of the error. This viewpoint was adopted in [3], where Corollary 4.15 was shown for the case that Γ is approximated by an interpolating spline of degree p. An alternative viewpoint is to ask whether it is possible to construct, by postprocessing u_h, an approximation $\widetilde{u}_h$ that is closer to u on S_δ than u_h. Indeed, it is possible to "extrapolate" the approximation $u_h|_{\Omega\setminus S_\delta}$ to the tubular neighborhood S_δ to arrive at a non-conforming approximation $\widetilde{u}_h$ ($\widetilde{u}_h$ is not necessarily in $H^1(\Omega)$). This is the approach taken in [4] for the case $p = 1$.

5 Numerical examples

In this section, we present five numerical examples to confirm the theoretical prediction of the convergence theory developed in Sections 2–4. All our numerical experiments are implemented in MATLAB. We test the affine linear finite element, subparametric, isoparametric and superparametric quadratic finite elements, which are denoted by P_1 ($m = 1$, $p = 1$), P_2 ($m = 1$, $p = 2$), $isoP_2$ ($m = 2$, $p = 2$) and $superP_2$ ($m = 3$, $p = 2$), respectively. In all calculations, we use interface-aligned triangulations, i.e., each element K of the triangulation satisfies either $\overline{K}\cap\Gamma = \emptyset$ or, otherwise, either a single vertex of K lies on the interface Γ or all the nodal points of one edge (or one face) of K lie on Γ. Note that after each mesh refinement, some regularly refined elements near the interface have to be slightly adjusted to ensure that they are interface-aligned. One way to ensure this is to use the functions `initmesh` and `refinemesh` in MATLAB's PDE toolbox.

Example 5.1. The computational domain Ω is $(-2,2)\times(-2,2)$, and the interface Γ is the unit circle $\{(x,y);\ x^2+y^2=1\}$. The exact solution u is chosen to be

$$u(x,y)=\begin{cases}\dfrac{1-(x^2+y^2)^2}{4\alpha_1}, & \text{if } x^2+y^2\leq 1;\\ \dfrac{1-(x^2+y^2)^2}{4\alpha_2}, & \text{if } x^2+y^2>1,\end{cases} \tag{49}$$

which has vanishing jumps both in the solution and the co-normal derivative Γ. The exact solution is shown in Figure 4 (a). Here we choose $\alpha_1 = 1$, $\alpha_2 = 10$, and define the source functions f and g through the equations (1) and (3) using the exact solution.

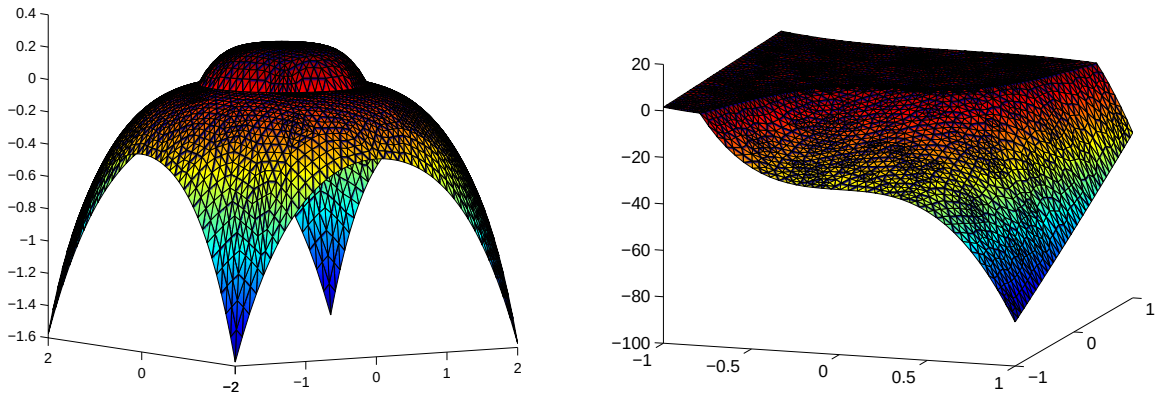

(a) (b)

Figure 4: (a): The exact solution in Example 5.1; (b): The exact solution in Example 5.2.

Figure 5 shows the convergence behavior of the P_1, P_2, $isoP_2$, and $superP_2$ elements. In Figure 5 (a), we can clearly see that the linear finite element P_1 gives the optimal first order convergence in the H^1-norm and second order convergence in the L^2-norm for $\delta = O(h^2)$. As the theory predicts, the affine-equivalent quadratic finite element P_2, can achieve only first order convergence in the H^1-norm and second order convergence in the L^2-norm due to the poor approximation of the interface ($\delta = O(h^2)$); see Figure 5 (b). In other words, only a small gain in accuracy is obtained by using P_2 elements instead of linear P_1 elements. Figure 5 (c) shows the convergence of $isoP_2$ elements. We observe second order convergence in the H^1-norm, which is better than $O(h^{3/2})$ predicted by Theorem 4.8. However, this effect is explained by symmetry properties of the circular interface, namely, a piecewise quadratic spline interpolating a circle leads to $\delta = O(h^4)$ instead of $\delta = O(h^3)$ for arbitrary (smooth) curves. For the superparametric quadratic finite element $superP_2$, the interface approximation order $\delta = O(h^4)$. Theory predicts the optimal second order convergence in the H^1-norm and third order convergence in the L^2-norm, and these are confirmed by the numerics in Figure 5 (d).

Example 5.2. The computational domain is $(-1,1)\times(-1,1)$ and the interface Γ is taken to be the cubic curve $y = 2x^3$. The exact solution u is given by

$$u(x,y) = \begin{cases} \dfrac{(y-2x^3)^2 - 30(y-2x^3)}{\alpha_1}, & \text{if } y \geq 2x^3; \\ \dfrac{(y-2x^3)^2 - 30(y-2x^3)}{\alpha_2}, & \text{if } y < 2x^3. \end{cases} \tag{50}$$

In our numerical test we have chosen $\alpha_1 = 20$, $\alpha_2 = 1$. The exact solution is shown in Figure 4 (b).

Figure 6 shows the numerical results for this example. As in Example 5.1, the convergence behavior of the P_1, P_2 and $superP_2$ elements confirm the theoretical prediction as shown in

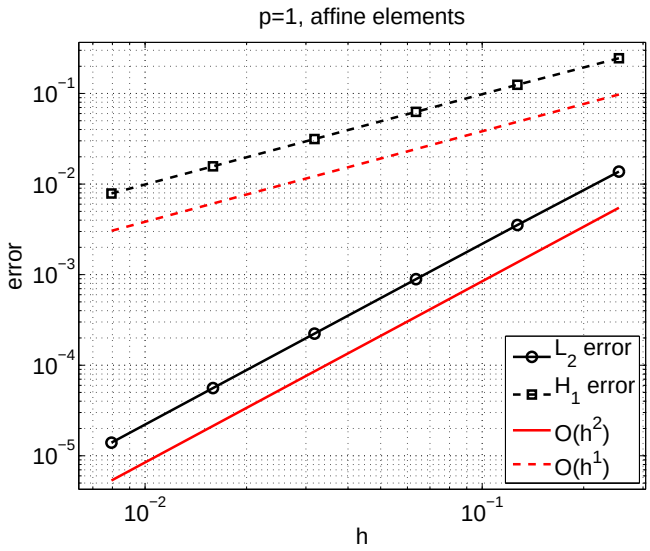

(a) P_1

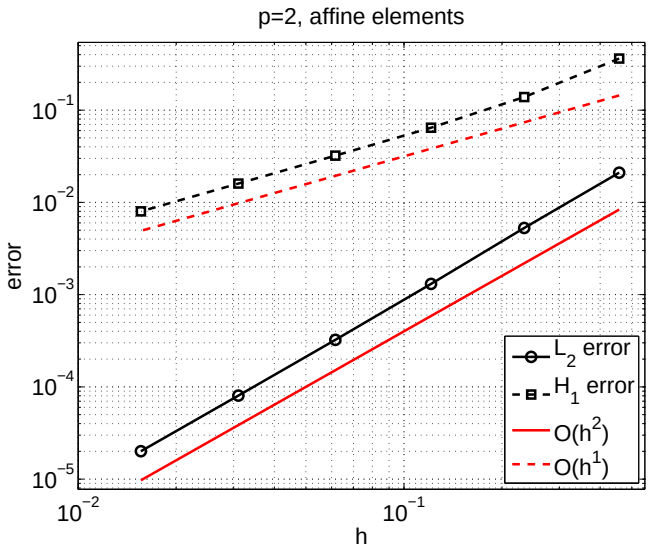

(b) P_2

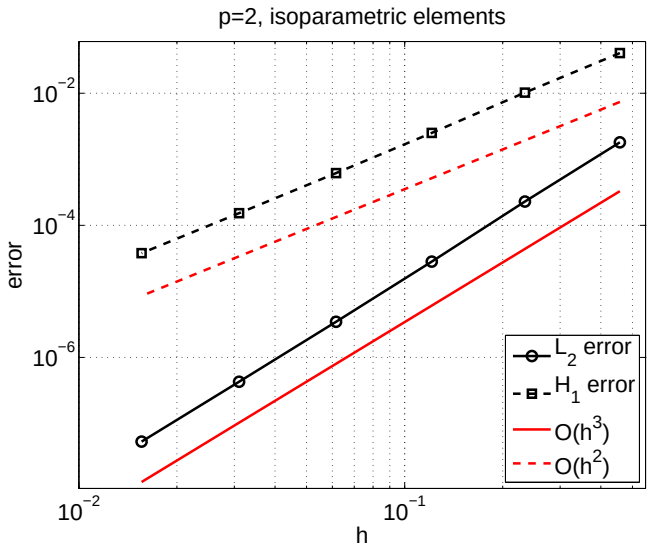

(c) $isoP_2$

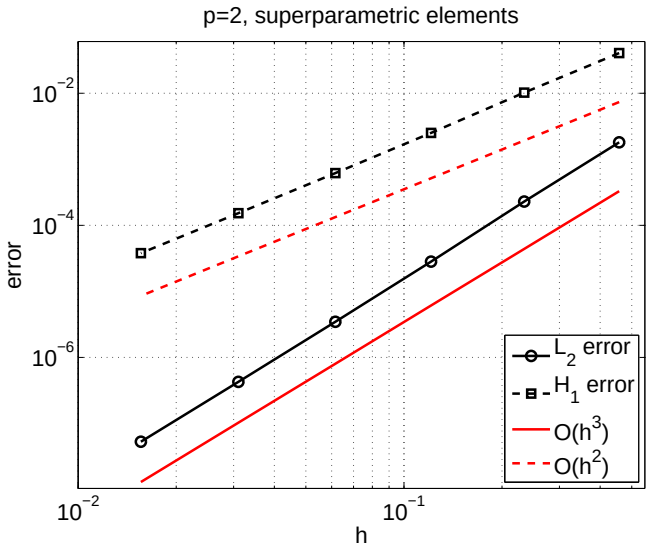

(d) $superP_2$

Figure 5: Convergence of P_1, P_2, $isoP_2$, and $superP_2$ elements in Example 5.1.

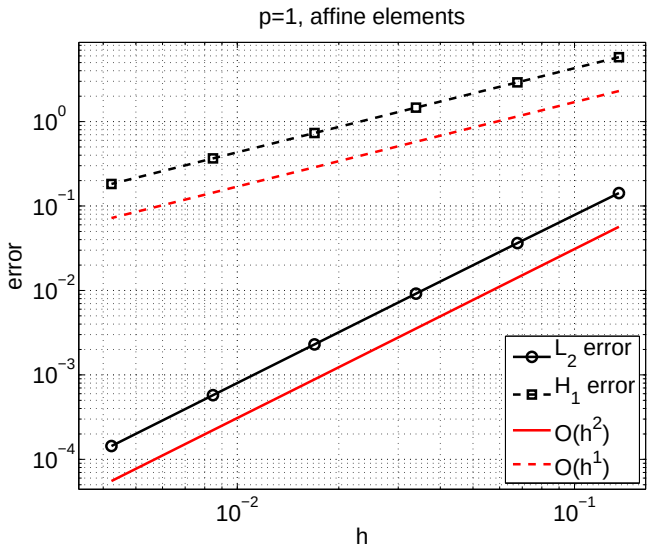

(a) P_1

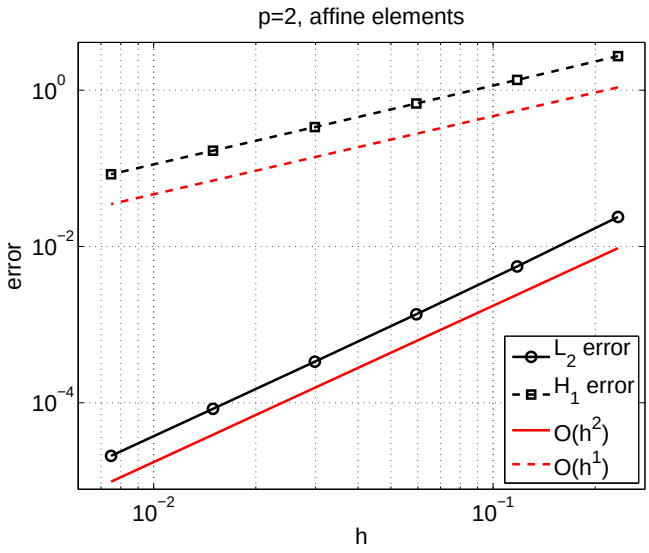

(b) P_2

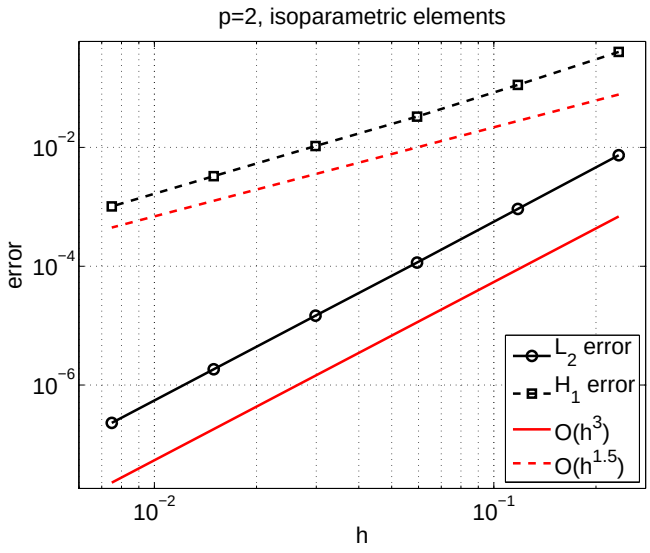

(c) $isoP_2$

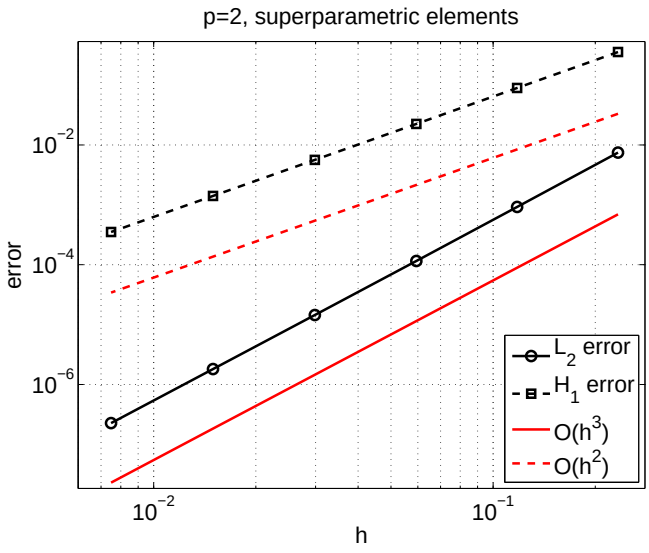

(d) $superP_2$

Figure 6: Convergence of P_1, P_2, $isoP_2$, $superP_2$ elements in Example 5.2.

Figure 6(a), (b) and (d). For the $isoP_2$ case, one does not obtain the optimal convergence rate due to the poor interface approximation $\delta = O(h^3)$. In Figure 6(c) the H^1-error appears to decay faster than the red reference line with slope 1.5. This is a preasymptotic phenomenon, since the global error consists of an $O(h^{1.5})$ contribution from relatively few elements near the interface and an $O(h^2)$ contribution from the elements away from the interface. Table 1 shows this in more detail, where the H^1-norms of the error $e = u - u_h$ are listed for the mismatch region $S := (\Omega_{1,h} \setminus \Omega_1) \cup (\Omega_{2,h} \setminus \Omega_2)$ and the region $\Omega \setminus S$. Table 1 also includes the number of degrees of freedom (dofs), and the level of refinement (level). Linear regression for the $isoP_2$-case shows a decay rate of 1.9573 for the $H^1(\Omega \setminus S)$-error and 1.5511 for the $H^1(S)$-error, which is in good agreement with Corollary 4.15 and Theorem 4.2.

			$isoP_2$ element		P_2 element	
level	dofs	h	$\|e\|_{H^1(\Omega\setminus S_\delta)}$	$\|e\|_{H^1(S_\delta)}$	$\|e\|_{H^1(\Omega\setminus S_\delta)}$	$\|e\|_{H^1(S_\delta)}$
1	751	2.3333(−1)	3.5494(−1)	1.9452(−1)	5.0444(−1)	2.6823(+0)
2	2,917	1.1771(−1)	8.9432(−2)	6.8844(−2)	1.5378(−1)	1.3448(+0)
3	11,497	5.9414(−2)	2.2461(−2)	2.4198(−2)	4.9227(−2)	6.7303(−1)
4	45,649	2.9848(−2)	6.4511(−3)	8.3592(−3)	1.6388(−2)	3.3662(−1)
5	181,921	1.4960(−2)	1.6391(−3)	2.8461(−3)	5.6011(−3)	1.6831(−1)
6	726,337	7.4888(−3)	4.0571(−4)	9.2957(−4)	1.9445(−3)	8.3974(−2)

Table 1: H^1-performance for P_2 and $isoP_2$ finite elements in Example 5.2.

Example 5.3. The computational domain is $(-1,1)\times(-1,1)$ and the interface Γ is the ellipse given by $\frac{16x^2}{9} + 4y^2 = 1$. The exact solution u is chosen as

$$u(x,y) = \begin{cases} 10 - 10(x^2+y^2)^2, & \text{if } \frac{16x^2}{9} + 4x^2 \le 1; \\ 110 - 10(x^2+y^2)^2 - \frac{1600}{9}x^2 - 400y^2, & \text{if } \frac{16x^2}{9} + 4x^2 > 1. \end{cases} \tag{51}$$

The solution u has non-vanishing interface values, and we choose piecewise smooth coefficients $\alpha_1 = (-6220x^2 + 6561)/(180x^2 + 81)$, $\alpha_2 = 1$ in the numerical test. The exact solution is shown in Figure 7 (a).

The convergence results for P_1, P_2, $isoP_2$ and $superP_2$ elements are plotted in Figure 8(a), (b), (c) and (d). Once again the numerical results confirm the theoretical predictions. In particular, the suboptimal behavior of the $isoP2$ approximation (see Figure 8(c)) is more evident than that in Example 5.2.

For this example, we also study the convergence behavior away from the interface as analyzed in Theorem 4.14. In Fig. 9, we present the errors $\|u - u_h\|_{H^1(S)}$ and $\|u - u_h\|_{H^1(\Omega\setminus S)}$ for P_2 and $isoP_2$ elements and $S = (\Omega_{1,h} \setminus \Omega_1) \cup (\Omega_{2,h} \setminus \Omega_2)$. We note that the $H^1(S)$-error is very close to the $H^1(\Omega)$-error in Fig. 8. In fact, $H^1(\Omega \setminus S)$-error is of higher order compared to $H^1(S)$, and Theorem 4.14 allows us to quantify this. Applying Theorem 4.14 with $\delta = O(h^2)$ for the case P_2 and $\delta = O(h^3)$ for the case $isoP_2$ we get for the error for the error $\|u - u_h\|_{H^1(\Omega\setminus S_\delta)}$ the bounds $O(h^{1.25})$ and $O(h^2)$, respectively. Numerically, we observe in Fig. 9 convergence $O(h^{1.5})$ and $O(h^2)$, respectively.

Example 5.4. We consider the well-known benchmark test of a 2D elastic interface problem specified in Sukumar et al., [23]. The problem is radially symmetric with different material properties in concentric discs around the origin. The computational domain is $\{(x,y);\ x^2+y^2 <$

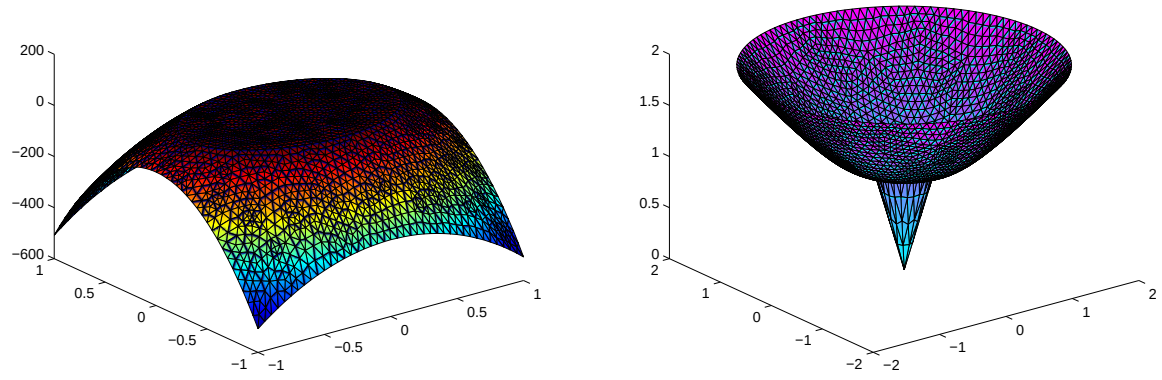

(a) (b)

Figure 7: (a): The exact solution in Example 5.3. (b): The exact solution in Example 5.4.

$b^2\}$ with a circular interface Γ of the form $x^2 + y^2 = a^2$. The inner disc has Young's modulus E_1 and Poisson ratio ν_1, and the outer one E_2 and ν_2. At any point, the displacement vector can be written as $\mathbf{u} = (u^r, u^\theta)$, where u^r is the radial component and u^θ is the circumferential component of the displacement. The material is subjected to the Dirichlet boundary condition $\mathbf{u} = \mathbf{x}$ (in Cartesian coordinates), and the exact solution to the problem is given by

$$u^r(r) = \begin{cases} \left(\left(1 - \frac{b^2}{a^2}\right)c + \frac{b^2}{a^2}\right) r, & 0 \le r \le a; \\ \left(r - \frac{b^2}{r}\right)c + \frac{b^2}{r}, & a \le r \le b. \end{cases}$$

with

$$c = \frac{(\lambda_1 + \mu_1 + \mu_2)b^2}{(\lambda_2 + \mu_2)a^2 + (\lambda_1 + \mu_1)(b^2 - a^2) + \mu_2 b^2}.$$

The Lamé constants λ_i and μ_i are given by $\lambda_i = \frac{E_i \nu_i}{(1+\nu_i)(1-2\nu_i)}$ and $\mu_i = \frac{E_i}{2(1+\nu_i)}$, $i = 1, 2$. Following [23], we select $E_1 = 1$, $\nu_1 = 0.25$, $E_2 = 10$, $\nu_2 = 0.3$, $a = 0.4$ and $b = 2$. The magnitude of the displacement of the exact solution are shown in Figure 7 (b).

Figure 10 displays the errors in the H^1- and L^2-norm as a function of the mesh size h. We clearly see that the linear elements P_1 achieves optimal convergence, i.e., first order in the H^1-norm and second order in the L^2-norm.

Example 5.5. Our last example is a 3D interface problem. We take the cubic domain $(-1, 1)^3$ as the computational domain with a spherical interface Γ: $x^2 + y^2 + z^2 = 0.7^2$. The exact solution u is given by

$$u(x, y) = \begin{cases} (0.7^2 - x^2 - y^2 - z^2)^2/\alpha_1, & \text{if } x^2 + y^2 + z^2 \le 0.7^2; \\ (0.7^2 - x^2 - y^2 - z^2)^2/\alpha_2, & \text{if } x^2 + y^2 + z^2 > 0.7^2, \end{cases} \tag{52}$$

with the discontinuous coefficients chosen to be $\alpha_1 = 1$ and $\alpha_2 = 10$ in our test, and is visualized with five equidistant slices along the x-axis in Figure 11 with a colormap nearby indicating the values of u.

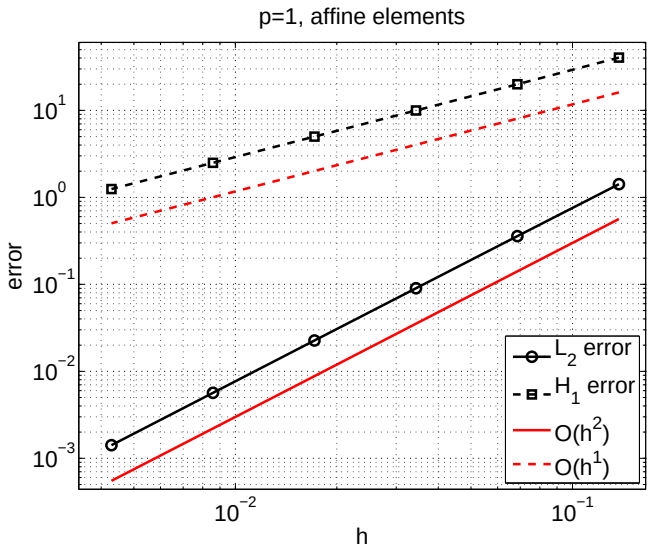

(a) P_1

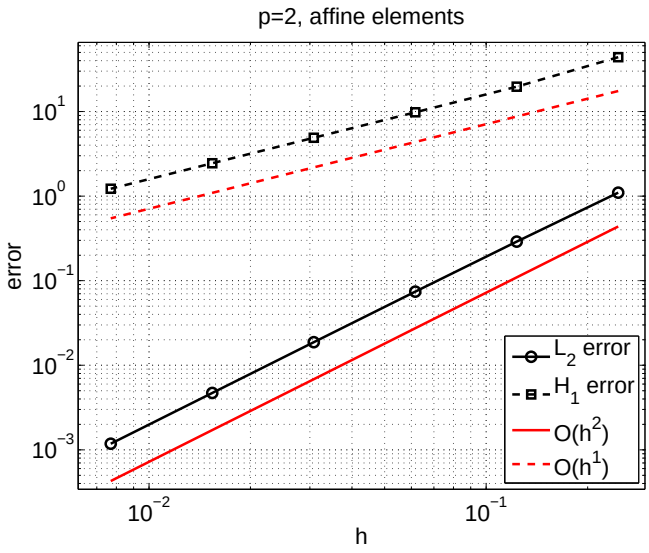

(b) P_2

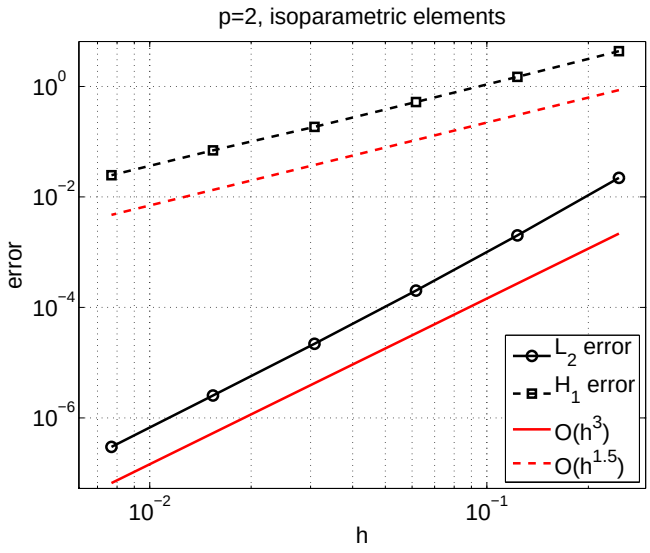

(c) $isoP_2$

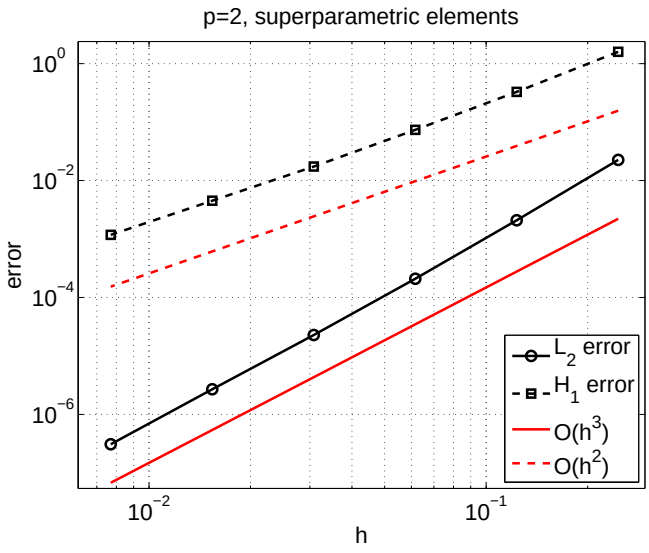

(d) $superP_2$

Figure 8: Convergence of P_1, P_2, $isoP_2$, $superP2$ elements for Example 5.3.

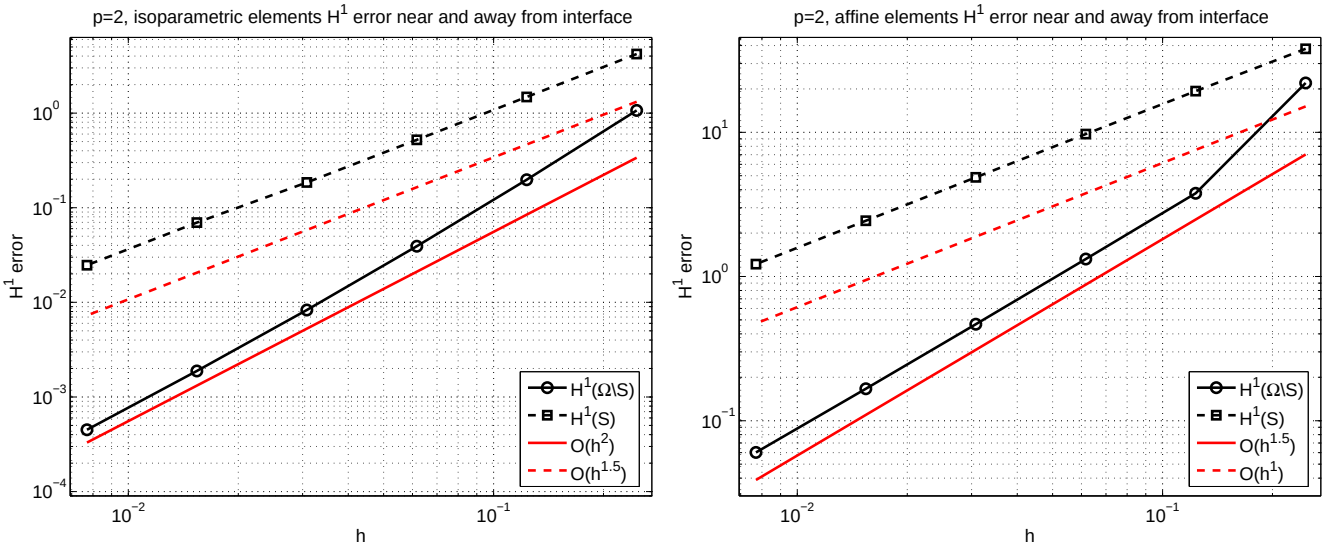

Figure 9: Example 5.3: Convergence in $H^1(\Omega \setminus S)$ and $H^1(S)$ with $S = (\Omega_{1,h} \setminus \Omega_1) \cup (\Omega_{2,h} \setminus \Omega_2)$. Left: isoparametric elements, $p = 2$. Right: affine elements $p = 2$.

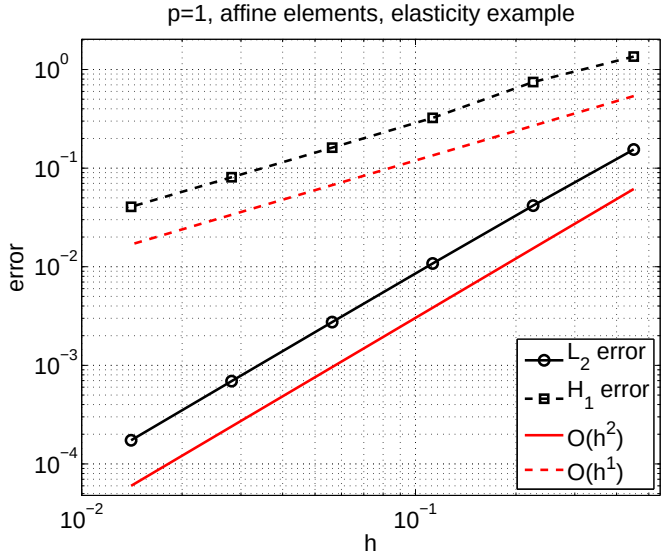

Figure 10: Convergence of P_1 finite elements for Example 5.4.

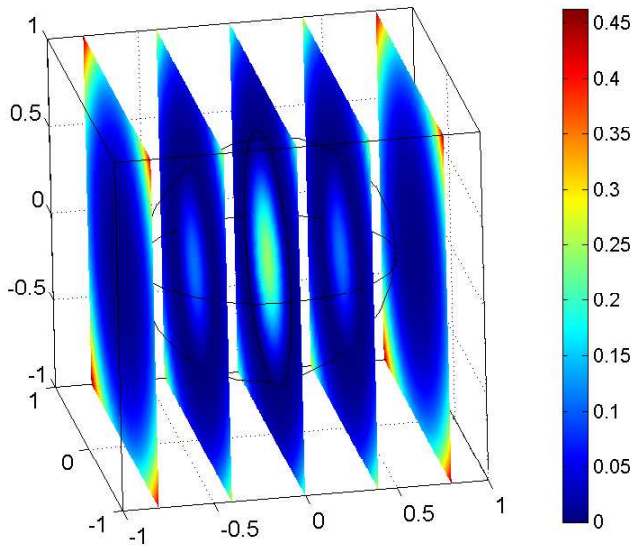

Figure 11: The exact solution in Example 5.5.

One can observe in Figure 12 that the linear finite elements P_1 yield optimal convergence in both the L^2 and H^1-norm as the mesh is refined. We mention that the final mesh has approximately $300,000$ vertices after five successive refinements.

6 Concluding remarks

This work is concerned with higher order finite element methods for solving the elliptic interface problems in d dimensions. A general convergence theory is developed for finite element methods in an abstract framework. A novel analysis tool is used for the error estimates of finite element interpolations for piecewise smooth functions. The tool, in combination with a *δ-strip* argument, enables us to improve the existing nearly optimal convergence of the continuous piecewise linear finite elements in two dimensions, and achieve the optimal convergence in three dimensions and for higher order finite elements. The new arguments reveal that not only the order of the finite elements must be increased but also the approximation of the interface should be improved to a certain degree in order to achieve a desired optimal higher order accuracy in H^1- and/or L^2-norm. Five concrete examples of the finite element methods for elliptic and elastic interface problems are numerically tested and compared, which confirm quite well the predictions and sharpness of the theory.

Acknowledgments

We are very grateful to two anonymous referees for their constructive comments. The research work leading to this paper was initiated during a stay of the first author at the IANS, University of Stuttgart; hence the first author wishes to express his special thanks to the hospitality of the third author.

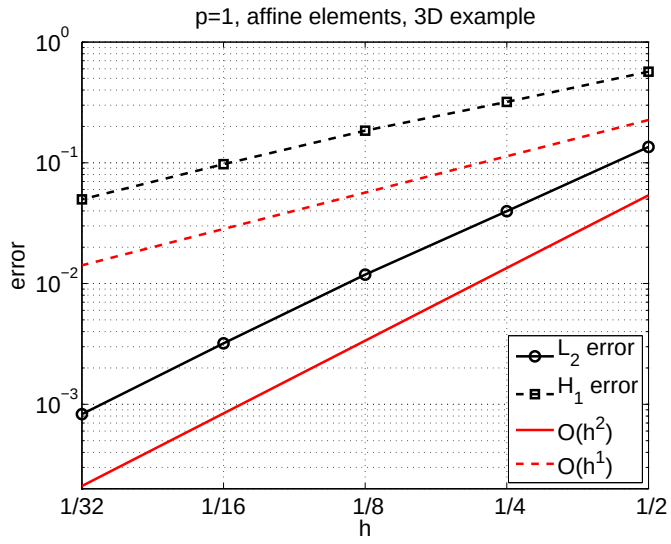

Figure 12: Convergence of P_1 finite elements for Example 5.5.

A Numerical results

For the purpose of comparison, we list in this appendix the relevant data of all the experiments in Section 5, including the number of uniform refinements R_N, the number of degrees of freedom `dofs`, the mesh size h, and various errors for the 5 examples. We set

$$S = (\Omega_{1,h} \setminus \Omega_1) \cup (\Omega_{2,h} \setminus \Omega_2).$$

Seven kinds of errors are calculated:

1. the $L^2(\Omega \setminus S)$ and $H^1(\Omega \setminus S)$ errors are denoted EN_L and EN_H, respectively ("N" for **non-interface**)
2. the $L^2(S)$ and $H^1(S)$ errors are denoted ES_L and ES_H respectively ("S" for **Strip**)
3. the **total** $L^2(\Omega)$ and $H^1(\Omega)$ errors are denoted ET_L and ET_H
4. the maximal nodal error is denoted L^∞.

R_N	dofs	h	EN_L	EN_H	ES_L	ES_H	ET_L	ET_H	L^∞
1	7.1000e+002	2.5441e-001	1.3732e-002	2.0522e-001	2.4281e-004	1.3350e-001	1.3734e-002	2.4482e-001	4.2998e-003
2	2.7570e+003	1.2721e-001	3.5297e-003	1.0486e-001	3.0342e-005	6.7377e-002	3.5298e-003	1.2464e-001	1.5450e-003
3	1.0865e+004	6.3603e-002	8.9067e-004	5.2817e-002	3.7900e-006	3.3801e-002	8.9067e-004	6.2707e-002	5.1061e-004
4	4.3137e+004	3.1801e-002	2.2332e-004	2.6470e-002	4.7351e-007	1.6923e-002	2.2332e-004	3.1417e-002	1.5806e-004
5	1.7191e+005	1.5901e-002	5.5879e-005	1.3244e-002	5.9171e-008	8.4665e-003	5.5879e-005	1.5719e-002	4.7025e-005
6	6.8634e+005	7.9503e-003	1.3973e-005	6.6234e-003	7.3951e-009	4.2344e-003	1.3973e-005	7.8612e-003	1.3628e-005

Table 2: History of error decay for P_1 finite element in Example 5.1.

References

[1] R. A. Adams. *Sobolev Spaces.* Academic Press, New York; London, 1975.

R_N	dofs	h	EN_L	EN_H	ES_L	ES_H	ET_L	ET_H	L^∞
1	7.3300e+002	4.5743e-001	2.0939e-002	2.6235e-001	1.8582e-003	2.4993e-001	2.1021e-002	3.6234e-001	1.6289e-002
2	2.8490e+003	2.3385e-001	5.2690e-003	5.6050e-002	2.3789e-004	1.2700e-001	5.2744e-003	1.3882e-001	4.1815e-003
3	1.1233e+004	1.2110e-001	1.3054e-003	8.9928e-003	2.9923e-005	6.3797e-002	1.3058e-003	6.4427e-002	1.0535e-003
4	4.4609e+004	6.1576e-002	3.2373e-004	3.1953e-003	3.7470e-006	3.1943e-002	3.2375e-004	3.2102e-002	2.6396e-004
5	1.7779e+005	3.1042e-002	8.0530e-005	1.1322e-003	4.6863e-007	1.5979e-002	8.0531e-005	1.6019e-002	6.6037e-005
6	7.0989e+005	1.5584e-002	2.0078e-005	4.0069e-004	5.8590e-008	7.9909e-003	2.0078e-005	8.0009e-003	1.6514e-005

Table 3: History of error decay for P_2 finite element in Example 5.1.

R_N	dofs	h	EN_L	EN_H	ES_L	ES_H	ET_L	ET_H	L^∞
1	7.3300e+002	4.5743e-001	1.8043e-003	3.8851e-002	9.4987e-007	1.1282e-002	1.8043e-003	4.0456e-002	1.1859e-003
2	2.8490e+003	2.3385e-001	2.2908e-004	9.8305e-003	2.5428e-008	2.7080e-003	2.2908e-004	1.0197e-002	1.7868e-004
3	1.1233e+004	1.2110e-001	2.8212e-005	2.4109e-003	5.8764e-010	6.9249e-004	2.8212e-005	2.5084e-003	2.6614e-005
4	4.4609e+004	6.1576e-002	3.4641e-006	5.9157e-004	1.3713e-011	1.7349e-004	3.4641e-006	6.1649e-004	3.6552e-006
5	1.7779e+005	3.1042e-002	4.2773e-007	1.4609e-004	3.3261e-013	4.3519e-005	4.2773e-007	1.5243e-004	4.7914e-007
6	7.0989e+005	1.5584e-002	5.3088e-008	3.6267e-005	8.5407e-015	1.0880e-005	5.3088e-008	3.7863e-005	6.1327e-008

Table 4: History of error decay for $isoP_2$ finite element in Example 5.1.

R_N	dofs	h	EN_L	EN_H	ES_L	ES_H	ET_L	ET_H	L^∞
1	7.3300e+002	4.5743e-001	1.8067e-003	3.8902e-002	5.8447e-005	1.1056e-002	1.8076e-003	4.0442e-002	1.1593e-003
2	2.8490e+003	2.3385e-001	2.2919e-004	9.8336e-003	4.0799e-006	2.7853e-003	2.2923e-004	1.0220e-002	1.8058e-004
3	1.1233e+004	1.2110e-001	2.8216e-005	2.4111e-003	2.6305e-007	6.9851e-004	2.8217e-005	2.5102e-003	2.6731e-005
4	4.4609e+004	6.1576e-002	3.4643e-006	5.9159e-004	1.6666e-008	1.7500e-004	3.4643e-006	6.1693e-004	3.6625e-006
5	1.7779e+005	3.1042e-002	4.2773e-007	1.4609e-004	1.0289e-009	4.3804e-005	4.2773e-007	1.5251e-004	4.7959e-007
6	7.0989e+005	1.5584e-002	5.3088e-008	3.6267e-005	6.3275e-011	1.0958e-005	5.3088e-008	3.7886e-005	6.1355e-008

Table 5: History of error decay for $superP_2$ finite element in Example 5.1.

R_N	dofs	h	EN_L	EN_H	ES_L	ES_H	ET_L	ET_H	L^∞
1	7.1900e+002	1.3548e-001	1.4236e-001	5.6168e+000	8.6498e-005	1.3901e+000	1.4236e-001	5.7863e+000	9.9619e-002
2	2.7910e+003	6.7741e-002	3.6386e-002	2.8362e+000	1.0821e-005	6.8440e-001	3.6386e-002	2.9176e+000	3.8003e-002
3	1.0997e+004	3.3870e-002	9.1713e-003	1.4236e+000	1.3530e-006	3.3946e-001	9.1713e-003	1.4635e+000	1.2806e-002
4	4.3657e+004	1.6935e-002	2.2990e-003	7.1277e-001	1.6915e-007	1.6902e-001	2.2990e-003	7.3254e-001	4.0108e-003
5	1.7397e+005	8.4676e-003	5.7524e-004	3.5654e-001	2.1138e-008	8.4151e-002	5.7524e-004	3.6633e-001	1.2034e-003
6	6.9456e+005	4.2338e-003	1.4385e-004	1.7829e-001	2.3808e-009	3.9000e-002	1.4385e-004	1.8251e-001	3.5092e-004

Table 6: History of error decay for P_1 finite element in Example 5.2.

R_N	dofs	h	EN_L	EN_H	ES_L	ES_H	ET_L	ET_H	L^∞
1	7.5100e+002	2.3333e-001	2.3840e-002	5.0444e-001	8.4971e-004	2.6823e+000	2.3855e-002	2.7293e+000	7.6624e-002
2	2.9170e+003	1.1771e-001	5.5507e-003	1.5378e-001	1.0633e-004	1.3448e+000	5.5518e-003	1.3536e+000	1.9378e-002
3	1.1497e+004	5.9414e-002	1.3550e-003	4.9227e-002	1.3296e-005	6.7303e-001	1.3551e-003	6.7483e-001	4.8680e-003
4	4.5649e+004	2.9848e-002	3.3590e-004	1.6388e-002	1.6622e-006	3.3662e-001	3.3590e-004	3.3702e-001	1.2196e-003
5	1.8192e+005	1.4960e-002	8.3700e-005	5.6011e-003	2.0777e-007	1.6831e-001	8.3700e-005	1.6840e-001	3.0520e-004
6	7.2634e+005	7.4888e-003	2.0896e-005	1.9445e-003	2.5961e-008	8.3974e-002	2.0896e-005	8.3996e-002	7.6334e-005

Table 7: History of error decay for P_2 finite element in Example 5.2.

R_N	dofs	h	EN_L	EN_H	ES_L	ES_H	ET_L	ET_H	L^∞
1	7.5100e+002	2.3333e-001	7.4043e-003	3.5494e-001	6.3022e-007	1.9452e-001	7.4043e-003	4.0475e-001	5.6546e-003
2	2.9170e+003	1.1771e-001	9.2045e-004	8.9432e-002	2.5821e-008	6.8844e-002	9.2045e-004	1.1286e-001	6.8781e-004
3	1.1497e+004	5.9414e-002	1.1526e-004	2.2461e-002	1.0758e-009	2.4198e-002	1.1526e-004	3.3016e-002	8.9284e-005
4	4.5649e+004	2.9848e-002	1.4745e-005	6.4511e-003	4.0205e-011	8.3592e-003	1.4745e-005	1.0559e-002	1.1291e-005
5	1.8192e+005	1.4960e-002	1.8433e-006	1.6391e-003	7.3168e-013	2.8461e-003	1.8433e-006	3.2843e-003	1.4150e-006
6	7.2634e+005	7.4888e-003	2.3051e-007	4.0571e-004	3.9317e-015	9.2957e-004	2.3051e-007	1.0142e-003	1.7698e-007

Table 8: History of error decay for $isoP_2$ finite element in Example 5.2.

R_N	dofs	h	EN_L	EN_H	ES_L	ES_H	ET_L	ET_H	L^∞
1	7.5100e+002	2.3333e-001	7.4664e-003	3.5729e-001	1.5782e-012	6.7137e-007	7.4664e-003	3.5729e-001	8.1278e-003
2	2.9170e+003	1.1771e-001	9.2471e-004	8.9760e-002	1.2424e-013	6.3858e-007	9.2471e-004	8.9760e-002	9.5602e-004
3	1.1497e+004	5.9414e-002	1.1553e-004	2.2497e-002	1.0591e-014	6.9782e-007	1.1553e-004	2.2497e-002	1.2163e-004
4	4.5649e+004	2.9848e-002	1.4458e-005	5.6308e-003	1.0723e-015	7.7674e-007	1.4458e-005	5.6308e-003	1.5319e-005
5	1.8192e+005	1.4960e-002	1.8087e-006	1.4081e-003	7.1763e-017	5.3385e-007	1.8087e-006	1.4081e-003	1.9072e-006
6	7.2634e+005	7.4888e-003	2.2619e-007	3.5213e-004	2.0294e-018	5.1592e-007	2.2619e-007	3.5213e-004	2.3989e-007

Table 9: History of error decay for $superP_2$ finite element in Example 5.2.

R_N	dofs	h	EN_L	EN_H	ES_L	ES_H	ET_L	ET_H	L^∞
1	7.1900e+002	1.3548e-001	1.4236e-001	5.6168e+000	8.6498e-005	1.3901e+000	1.4236e-001	5.7863e+000	9.9619e-002
2	2.7910e+003	6.7741e-002	3.6386e-002	2.8362e+000	1.0821e-005	6.8440e-001	3.6386e-002	2.9176e+000	3.8003e-002
3	1.0997e+004	3.3870e-002	9.1713e-003	1.4236e+000	1.3530e-006	3.3946e-001	9.1713e-003	1.4635e+000	1.2806e-002
4	4.3657e+004	1.6935e-002	2.2990e-003	7.1277e-001	1.6915e-007	1.6902e-001	2.2990e-003	7.3254e-001	4.0108e-003
5	1.7397e+005	8.4676e-003	5.7524e-004	3.5654e-001	2.1138e-008	8.4151e-002	5.7524e-004	3.6633e-001	1.2034e-003
6	6.9456e+005	4.2338e-003	1.4385e-004	1.7829e-001	2.3808e-009	3.9000e-002	1.4385e-004	1.8251e-001	3.5092e-004

Table 10: History of error decay for P_1 finite element in Example 5.3.

R_N	dofs	h	EN_L	EN_H	ES_L	ES_H	ET_L	ET_H	L^∞
1	6.9300e+002	2.4652e-001	1.0908e+000	2.2000e+001	1.4236e-001	3.7969e+001	1.1001e+000	4.3882e+001	1.1504e+000
2	2.6890e+003	1.2326e-001	2.8950e-001	3.7784e+000	1.9147e-002	1.9315e+001	2.9013e-001	1.9681e+001	3.1339e-001
3	1.0593e+004	6.1631e-002	7.4152e-002	1.3219e+000	2.4658e-003	9.7184e+000	7.4193e-002	9.8079e+000	8.0853e-002
4	4.2049e+004	3.0815e-002	1.8743e-002	4.6684e-001	3.1232e-004	4.8716e+000	1.8746e-002	4.8939e+000	2.0535e-002
5	1.6755e+005	1.5408e-002	4.7103e-003	1.6651e-001	3.9280e-005	2.4385e+000	4.7104e-003	2.4442e+000	5.2264e-003
6	6.6893e+005	7.7038e-003	1.1806e-003	6.0217e-002	4.9246e-006	1.2199e+000	1.1806e-003	1.2214e+000	1.3197e-003

Table 11: History of error decay for P_2 finite element in Example 5.3.

R_N	dofs	h	EN_L	EN_H	ES_L	ES_H	ET_L	ET_H	L^∞
1	6.9300e+002	2.4652e-001	2.2092e-002	1.0674e+000	3.4692e-004	4.2074e+000	2.2095e-002	4.3406e+000	4.5236e-002
2	2.6890e+003	1.2326e-001	2.0117e-003	1.9740e-001	1.5177e-005	1.4783e+000	2.0118e-003	1.4914e+000	5.7106e-003
3	1.0593e+004	6.1631e-002	2.0179e-004	3.9142e-002	6.6688e-007	5.2122e-001	2.0179e-004	5.2269e-001	7.2301e-004
4	4.2049e+004	3.0815e-002	2.1919e-005	8.2960e-003	2.9083e-008	1.8511e-001	2.1919e-005	1.8529e-001	9.1177e-005
5	1.6755e+005	1.5408e-002	2.5418e-006	1.8841e-003	1.7892e-009	6.9612e-002	2.5418e-006	6.9637e-002	1.2292e-005
6	6.6893e+005	7.7038e-003	2.9887e-007	4.5074e-004	8.1327e-011	2.4685e-002	2.9887e-007	2.4689e-002	1.7550e-006

Table 12: History of error decay for $isoP_2$ finite element in Example 5.3.

R_N	dofs	h	EN_L	EN_H	ES_L	ES_H	ET_L	ET_H	L^∞
1	6.9300e+002	2.4652e-001	2.2606e-002	1.1980e+000	1.5412e-005	1.0519e+000	2.2606e-002	1.5943e+000	8.4432e-002
2	2.6890e+003	1.2326e-001	2.0882e-003	2.1680e-001	5.6035e-007	2.4717e-001	2.0882e-003	3.2877e-001	9.2766e-003
3	1.0593e+004	6.1631e-002	2.0906e-004	4.1998e-002	2.7710e-008	6.0422e-002	2.0906e-004	7.3584e-002	1.0377e-003
4	4.2049e+004	3.0815e-002	2.2762e-005	8.8773e-003	1.6068e-009	1.4897e-002	2.2762e-005	1.7341e-002	2.2128e-004
5	1.6755e+005	1.5408e-002	2.6934e-006	2.0892e-003	1.0260e-010	4.0132e-003	2.6934e-006	4.5244e-003	2.6740e-005
6	6.6893e+005	7.7038e-003	3.0837e-007	4.9474e-004	2.1163e-013	1.0674e-003	3.0837e-007	1.1764e-003	2.8472e-006

Table 13: History of error decay for $superP_2$ finite element in Example 5.3.

R_N	dofs	h	EN_L	EN_H	ES_L	ES_H	ET_L	ET_H	L^∞
1	3.1200e+002	4.5021e-001	1.5013e-001	9.9602e-001	3.5685e-002	9.1427e-001	1.5431e-001	1.3520e+000	1.3021e-001
2	1.1740e+003	2.2511e-001	4.1359e-002	5.6411e-001	5.2191e-003	4.8873e-001	4.1687e-002	7.4638e-001	4.0213e-002
3	4.5540e+003	1.1255e-001	1.0765e-002	2.0238e-001	7.0400e-004	2.5209e-001	1.0788e-002	3.2327e-001	1.4732e-002
4	1.7938e+004	5.6277e-002	2.7441e-003	9.7970e-002	9.2300e-005	1.2807e-001	2.7457e-003	1.6124e-001	5.5225e-003
5	7.1202e+004	2.8138e-002	6.9200e-004	4.8683e-002	1.1889e-005	6.4566e-002	6.9211e-004	8.0863e-002	1.8986e-003
6	2.8371e+005	1.4069e-002	1.7358e-004	2.4283e-002	1.5121e-006	3.2420e-002	1.7358e-004	4.0506e-002	6.0919e-004

Table 14: History of error decay for P_1 finite element in Example 5.4.

[2] I. Babuška. The finite element method for elliptic equations with discontinuous coefficients. *Computing*, 5:207–213, 1970.

[3] J. W. Barrett and C. M. Elliott. Fitted and unfitted finite-element methods for elliptic equations with smooth interfaces. *IMA J. Numer. Anal.*, 7:283–300, 1987.

[4] J. H. Bramble and J. T. King. A finite element method for interface problems in domains with smooth boundaries and interfaces. *Adv. Comput. Math.*, 6:109–138, 1996.

[5] S. C. Brenner and L. R. Scott. *The mathematical theory of finite element methods.* Springer Verlag, second edition, 2002.

[6] E. Burman and P. Hansbo. Interior penalty stabilized Lagrange multiplier methods for the finite element solution of elliptic interface problems. *Preprint*, Finite Element Center, 2007.

[7] Z. Chen and J. Zou. Finite element methods and their convergence for elliptic and parabolic interface problems. *Numer. Math.*, 79:175–202, 1998.

[8] B. Camp, T. Lin, Y. Lin, and W. Su. Quadratic immersed finite element spaces and their approximation capabilities. *Adv. Comput. Math.*, 24:81–112, 2006.

[9] P. G. Ciarlet. *The Finite Element Method for Elliptic Problems.* Studies in Mathematics and its Applications. North-Holland Pub. Co., Amsterdam, New York, first edition, 1978.

[10] P. Grisvard. *Singularities in Boundary Value Problems.* Springer Verlag/Masson, 1992.

[11] W. J. Gordon. Blending-function methods of bivariate and multivariate interpolation and approximation. *SIAM J. Numer. Anal.*, 8(1):158–177, 1971.

[12] W. J. Gordon and C. A. Hall. Construction of curvilinear coordinate systems and application to mesh generation. *Internat. J. of Numer. Methods Engrg.*, 7:461–477, 1973.

[13] W. J. Gordon and C. A. Hall. Transfinite element methods: Blending-function interpolation over arbitrary curved element domains. *Numer. Math.*, 21(2):109–129, 1973.

[14] A. Hansbo and P. Hansbo. An unfitted finite element method, based on Nitsche's method, for elliptic interface problems. *Comput. Methods Appl. Mech. Engrg.*, 191(47):537–552, 2002.

[15] J. Huang and J. Zou. A mortar element method for elliptic problems with discontinuous coefficients. *IMA J Numer. Anal.*, 22:549–576, 2002.

[16] M. Lenoir. Optimal isoparametric finite elements and error estimates for domains involving curved boundaries. *SIAM J. Numer. Anal.*, 23:562–580, 1986.

[17] J. Li, J. M. Melenk, B. Wohlmuth and J. Zou. Convergence Analysis of Higher Order Finite Element Methods for Elliptic Interface Problems. *Technical report, TU Wien*, 2008.

[18] Z. Li, T. Lin, and X. Wu. New cartesian grid methods for interface problem using finite element formulation. *Numer. Math.*, 96:61–98, 2003.

[19] Z. Li and K. Ito. *The immersed interface method : numerical solutions of PDEs involving interfaces and irregular domains.* Philadelphia : Society for Industrial and Applied Mathematics, 2006.

[20] T. Lin, Y. Lin, and W. Sun. Error estimation of a class of quadratic immersed finite element methods for elliptic interface problems. *Disc. Cont. Dynam. Sys., Series B*, 7(4):807–823, 2007.

[21] M. Plum and C. Wieners. Optimal a priori estimates for interface problems. *Numer. Math.*, 95:735–759, 2003.

[22] E. M. Stein. *Singular integrals and differentiability properties of functions.* Princeton University Press, Princeton, 1970.

[23] N. Sukumar, D. L. Chopp, N. Noës, and T. Bleytschko. Modeling holes and inclusions by level sets in the extended finite-element method. *Comput. Methods Appl. Mech. Engrg.*, 190:6183–6200, 2001.

[24] O. C. Zienkiewicz and R. L. Taylor. *The Finite Element Method Vol. 1. The basis.* Oxford, Boston : Butterworth-Heinemann, fifth edition, 2000.